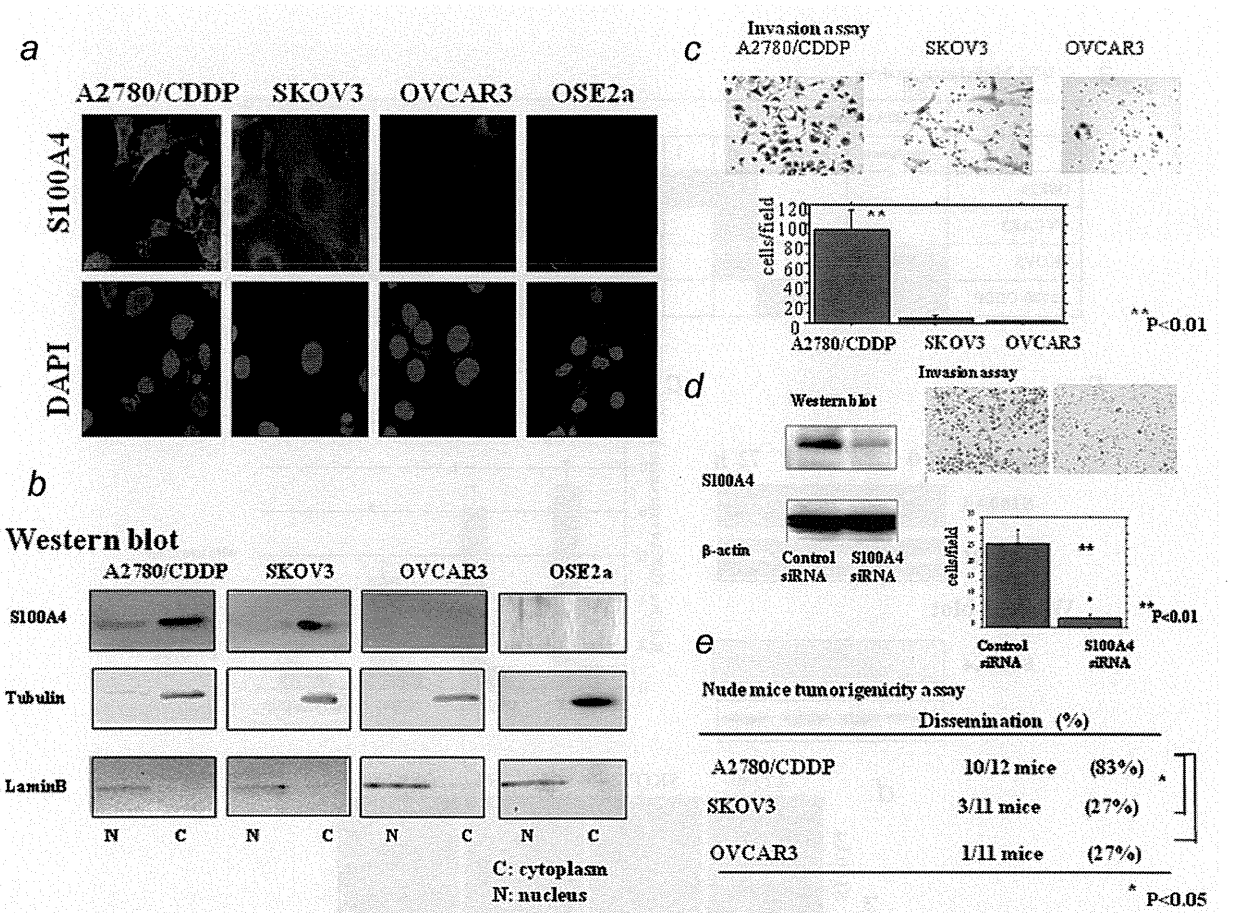

Figure 1. (*a*) Immunofluorescent analysis of S100A4 in ovarian carcinoma cell lines. Immunofluorescent staining of S100A4 showed diffuse staining in both the cytoplasm and nucleus in A2780/CDDP cells. In SKOV3 cells, diffuse staining of S100A4 was observed in the cytoplasm. In OVCAR3 and OSE2a cells, the expression of S100A4 was faint. Upper panel: S100A4 staining (red), Lower panel: Nuclei were counterstained with DAPI (blue). (*b*) Western blot analysis of the cytoplasmic and nuclear fractions. This analysis confirmed the subcellular expression pattern of S100A4 in 4 ovarian carcinoma cell lines. N: nuclear fraction and C: cytoplasmic fraction. (*c*) Matrigel invasion assay. The number of cells that passed through Matrigel-coated membranes was used to represent invasive activity. The Matrigel invasion assay showed that the invasive activity of A2780/CDDP cells, which express S100A4 in their nuclei, was significantly higher than those of SKOV3 and OVCAR3 cells. $*p < 0.05$. Student's *t*-test. (*d*) Matrigel invasion assay after the transfection of S100A4 siRNA. To confirm the role of S100A4 in invasiveness, we transfected S100A4 specific siRNA into A2780/CDDP cells. The reduction in S100A4 expression caused decreased invasiveness. $*p < 0.05$. Student's *t*-test. (*e*) Nude mouse tumorigenicity assay. We examined the tumor formation rate at 1 month after the intraperitoneal injection of the cells into nude mice. The frequency of nude mouse dissemination was correlated with the expression level of S100A4 in ovarian cancer cell lines tested. Individual disseminated tumors were evaluated by the percentage of tumor development among injected mice, described as the dissemination rate. The frequency of nude mouse dissemination was correlated with the expression level of S100A4 in all ovarian cancer cell lines tested.$*p < 0.05$. Fischer's exact test.

showed that the transcriptional activity of the S100A4 first intron was similar to that of endogenous S100A4 expression (Supporting Information Fig. 1). This sequence has 11 CpG sites (Supporting Information Fig. 1). Therefore, we investigated the association between the methylation statuses of these 11 CpG sites and the expression of S100A4 in ovarian carcinoma cells. The examination of sodium bisulfite-modified DNA showed that the hypomethylation of the CpG sites in the first intron is correlated with increased S100A4 expression (Fig. 2*a*).

To confirm the effect of CpG methylation on S100A4 expression *in vitro*, OVCAR3 cells were continuously exposed to 5Aza-dC. The expression of S100A4 was increased at both the mRNA and protein levels after 5-Aza-dC treatment in a time-dependent manner (Fig. 2*b*). Real-time RT-PCR showed that the S100A4 expression of OSE2a, OVCAR3 and SKOV3

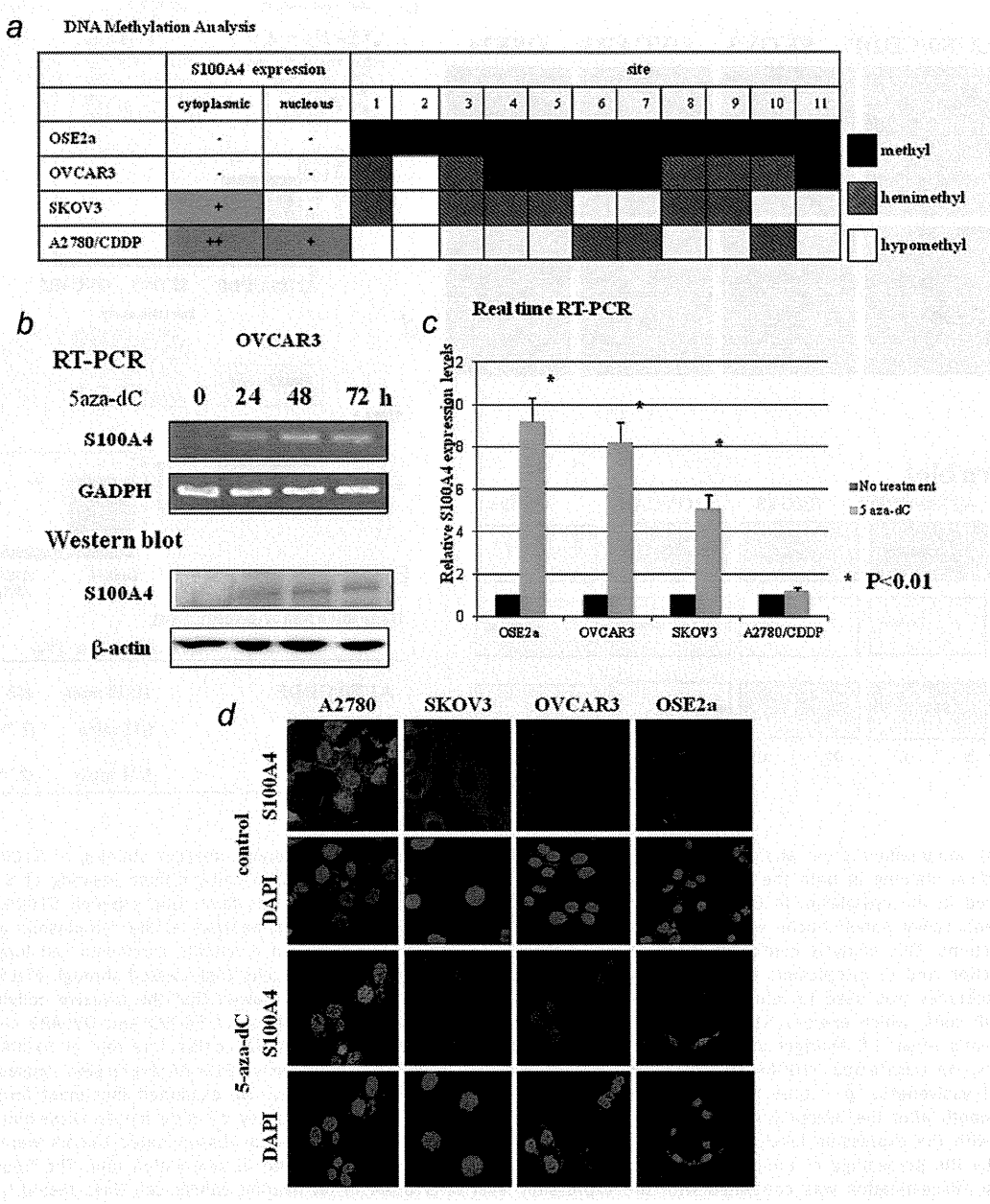

Figure 2. (*a*) DNA methylation analysis of S100A4 using sodium bisulfite sequencing. All 11 CpG sites of the first intron were methylated in OSE2a cells, which do not express S100A4. OVCAR3 cells showed very low endogenous expression of S100A4 mRNA and demonstrated that 10/11 sites were methylated or hemimethylated. A2780/CDDP cells, which have high endogenous levels of S100A4 mRNA, demonstrated that 8/11 sites were hypomethylated. The hypomethylation frequency was intermediate in SKOV3 cells. White: hypomethylated, gray: hemimethylated and black: methylated. (*b*) RT-PCR and Western blot analyses of the expression of S100A4 in OVCAR3 cells after 5-Aza-dC treatment. The expression of S100A4 was increased at both the mRNA and protein levels after 5-aza-dC treatment in a time-dependent manner. 5-aza-dC: 1 μM 5-aza-dC. (*c*) Changes in S100A4 mRNA expression after 5-Aza-dC treatment. The relative expression levels of S100A4 were estimated by real-time RT-PCR. The mRNA expression of S100A4 was increased after 5-aza-dC treatment in OSE2a, OVCAR3 and SKOV3. 5-aza-dC: 1 μM 5-aza-dC 96 hr, Values are the mean ± SD. *$p < 0.05$. Student's *t*-test. (*d*) Immunofluorescent analysis of S100A4 expression by treatment with 5-aza-dC. The changes of S100A4 localization after treatment with 5aza-dC were examined by immunofluorescence staining. 5-aza-dC treatment increased the nuclear expression of S100A4 in SKOV3, OVCAR3 and OSE2a. Upper panel: S100A4 staining (red), Lower panel: Nuclei were counterstained with DAPI (blue). 5-aza-dC: 1 μM 5-aza-dC for 96 hr.

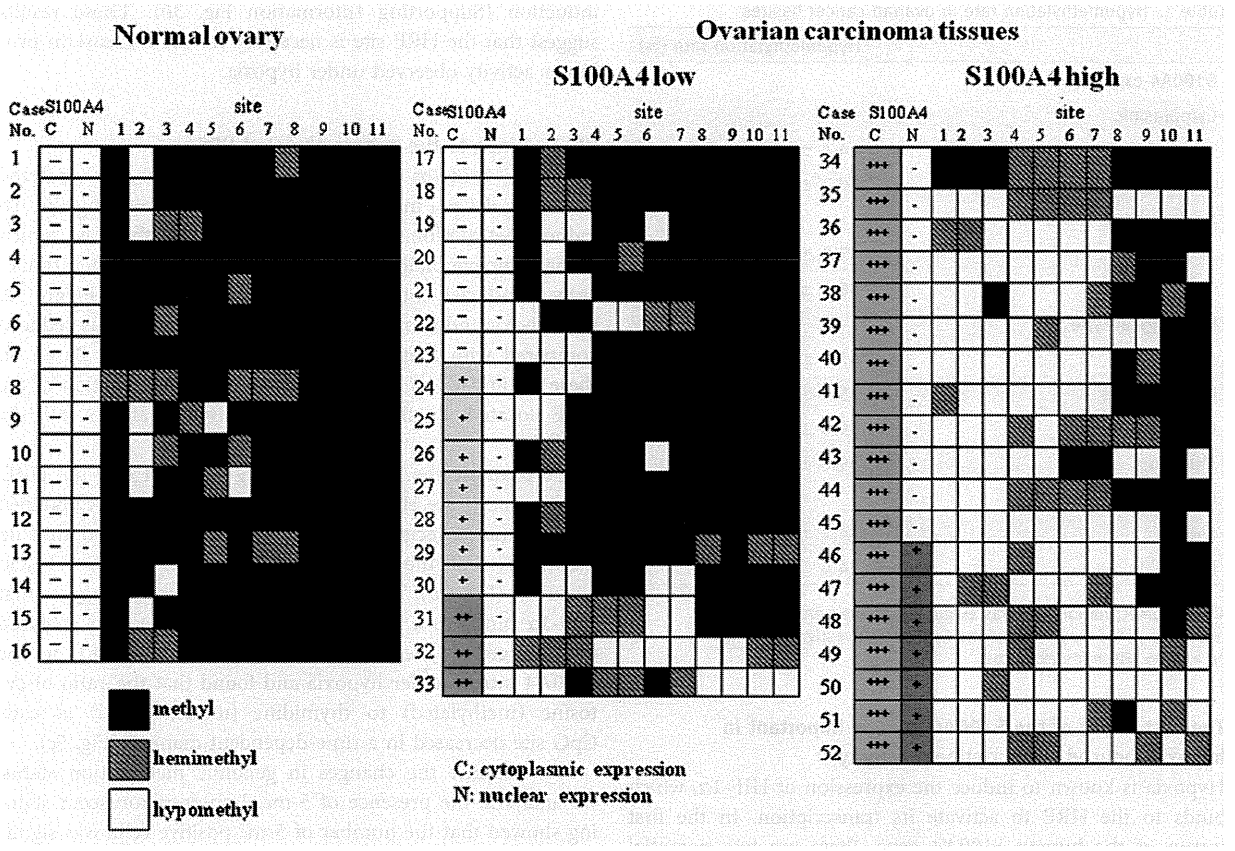

Figure 3. DNA methylation analysis of S100A4 in ovarian cancer tissues. S100A4 overexpression in ovarian cancer tissues showed a high frequency of hypomethylation. White: hypomethylation, gray: hemimethylation and black: methylation. N: nuclear S100A4 expression, C: cytoplasmic S100A4 expression.

cells was significantly increased by 5-aza-dC treatment (Fig. 2*c*); however, no significant difference was found in the density of the S100A4 band in the A2780/CDDP cells after either treatment (Fig. 2*c*). In addition, we examined the changes of S100A4 localization by treatment with 5-aza-dC by immunofluorescence staining. As shown in Figure 2*d*, 5-aza-dC treatment increased the nuclear expression of S100A4 in SKOV3, OVCAR3 and OSE2a. Thus, these results provide evidence that DNA methylation is an important regulatory mechanism for S100A4 expression in ovarian cancer cell lines.

Hypomethylation of the first intron of the S100A4 gene is correlated with increased S100A4 expression in ovarian cancer tissues

We investigated the association between S100A4 expression and methylation status in ovarian carcinoma tissues. The results are shown in Figure 3. S100A4 overexpression in ovarian cancer tissues showed the high frequency of hypomethylation (Table 1). Furthermore, according to the FIGO stage classification, the hypomethylation rate in Stages III and IV (54%) cases is significantly higher than that in stages I and II (34%, $p < 0.01$; Table 1). Therefore, epigenetic changes might be induced during ovarian cancer progression.

Hypoxia facilitates the invasiveness of ovarian carcinoma cells through S100SA4 upregulation

Next, we examined the effect of hypoxia on S100A4 expression in ovarian carcinoma cell lines, SKOV3, A2780/CDDP, OVCAR3 and OSE2a (Fig. 4*a* and Supporting Information Fig. 2). The nuclear expression of S100A4 was observed under hypoxia, whereas S100A4 expression was observed in the cytoplasm of SKOV3 cells under normoxia (Fig. 4*a*). Western blotting also revealed S100A4 expression in the nuclear compartment of SKOV3 cells under hypoxia (Fig. 4*b*). In addition, hypoxia resulted in increased invasiveness and induced the expression of S100A4 in SKOV3 cells (Fig. 4*c*). Furthermore, when S100A4 siRNA was transfected into ovarian carcinoma cells, hypoxia-induced invasive activity was reduced ($p < 0.05$; Fig. 4*c*). These findings suggest that the increased invasiveness of ovarian carcinoma cells observed under hypoxia is associated with the induction of S100A4 expression.

Table 1. Hypomethylation rate in ovarian cancer tissues

	Hypomethylation rate (%)
S100A4 expression	
Cytoplasmic	
−~+	14.4 ± 12.4
++~+++	50.3 ± 16.4*
Nuclear	
−	33.0 ± 17.3
+	68.1 ± 14.6*
Histological type	
Serous	47.8 ± 26.3
Endometrioid	35.1 ± 21.7
Clear cell	39.0 ± 26.3
Mucinous	39.6 ± 18.6
FIGO stage	
I+II	34.2 ± 26.7
III+IV	54.4 ± 25.1*

The hypomethylation rate was evaluated as the percentage of hypomethylated CpG in all of the CpG sites investigated.
*$p < 0.05$. Fischer's exact test.

The first intron of the S100A4 gene is important in hypoxia-induced transcriptional activity

Hypoxia is known to induce the expression of HIF-1α, which binds to the HRE to activate its transcription. In the first intron of the human S100A4 gene, there are two potential HIF binding sites, HRE1at position +196 and HRE2at position +329 (Fig. 4*d*). We made serial deletions in the S100A4 intron and produced the pLuc3(-4), pLuc3(248), pLuc3(383) and pLuc3(718) plasmids (Fig. 4*d*). Normalized luciferase activity was enhanced 9-fold and 7-fold in the SKOV3 cells transfected with pLuc3(-4) and pLuc3(248), respectively (Fig. 4*e*). In the OVCAR3 cells transfected with pLuc3(-4), it was enhanced 6-fold under hypoxia. Neither the pLuc3(383) construct nor the pLuc3(718) plasmid enhanced luciferase activity when the transfected cells were exposed to hypoxia (Fig. 4*e*).

We then analyzed the binding of HIF-1α to the HRE in the S100A4 intron under hypoxia using the ChIP assay. As shown in Figure 4*f*, increased HIF-1α DNA binding to HRE1 and HRE2 under hypoxia was observed in SKOV3 cells. OVCAR3 cells showed increased HIF-1α DNA binding to HRE1. The results of methylation analysis showed that HRE2 in OVCAR3 was methylated; therefore, we speculated that the methylation status is important for HIF-1α DNA binding to HRE under hypoxia. In support of the results of the ChIP assay, the suppression of HIF-1α expression by siRNA inhibited the transcriptional induction of S100A4 (Supporting Information Fig. 3*a*). In addition, S100A4 transcriptional activity of pLuc3(-4) under hypoxia was increased, but not that of the double mutant of HRE1 and HRE2. Both HRE1 and HRE2 were associated with the upregulation of S100A4 induction (Supporting Information Fig. 3*b*). These results suggest that the HRE site is necessary for the increase in promoter activity observed under hypoxia.

HIF-1α binds to the hypomethylated HRE

The HRE contains CpG dinucleotides.[35] Thus, we analyzed the effect of CpG methylation on the HIF-1α binding site. To induce methylation, pLuc3(-4) was treated with SAM, which is the principle biological methyl donor, and was then transiently transfected into A2780/CDDP. As shown in Figure 5*a*, the hypoxic inducibility of methylated pLuc3(-4) was reduced compared with that of SAM untreated pLuc3(-4). Based on these results, it was assumed that the CpG methylation of the HRE located in the S100A4 first intron affects HIF-1α binding.

To examine the impaired binding of HIF-1α to the HRE, we sequenced the HRE of the HIF-1α binding DNA obtained from immunoprecipitation. Our sequencing showed that no methylation of the HIF-1 binding region of S100A4 had occurred (Fig. 5*b*). Taken together, these results suggest that HIF-1α binds to a methylation-free HRE. We also analyzed the changes in the methylation status of the HRE in the S100A4 intron under hypoxia and found that the ratio of cytosine (methylated) to thymidine (unmethylated) at each CpG site decreased in a time-dependent manner (Fig. 5*c*).

To examine the changes in genomic methylation status, we analyzed the presence of 5-mc. Immunofluorescent staining showed that the number of 5-mc positive cells was significantly decreased under hypoxia ($p < 0.05$; Fig. 5*d*). As the methylation process depends on the balance of several factors, such as DNA methyltransferase (DNMT) enzymes and demethylases,[36,37] we examined the changes in DNMT activity and expression under hypoxia. Although different cell lines demonstrated different levels of DNMT activity, the OVCAR3 and SKOV3 cells lines showed reduced DNMT activity after being exposed to hypoxia (Fig. 5*e*). RT-PCR analysis showed that the mRNA expression of the maintenance methyltransferase DNMT1 was decreased under hypoxia in OVCAR3 cells (Fig. 5*f*). In contrast, there were no significant changes in the mRNA expression of the *de novo* methyltransferases DNMT3A and DNMT3B.

The coexpression of nuclear S100A4 and HIF-1α is correlated with the poor prognosis of ovarian carcinoma patients

Finally, we examined the importance of S100A4 and HIF-1α in patients with ovarian cancer. Among patients of all stages, the prognosis was significantly poorer in patients that demonstrated strong nuclear expression of S100A4 (positive, 43.1 ± 12.5 months *vs.* negative, 97.2 ± 8.3 months, $p = 0.005$). Interestingly, the coexpression of nuclear S100A4 and HIF-1α was associated with significantly shorter survival ($p < 0.0001$; Supporting Information Fig. 4). Accordingly, the nuclear expression of S100A4 combined with HIF-1α might be

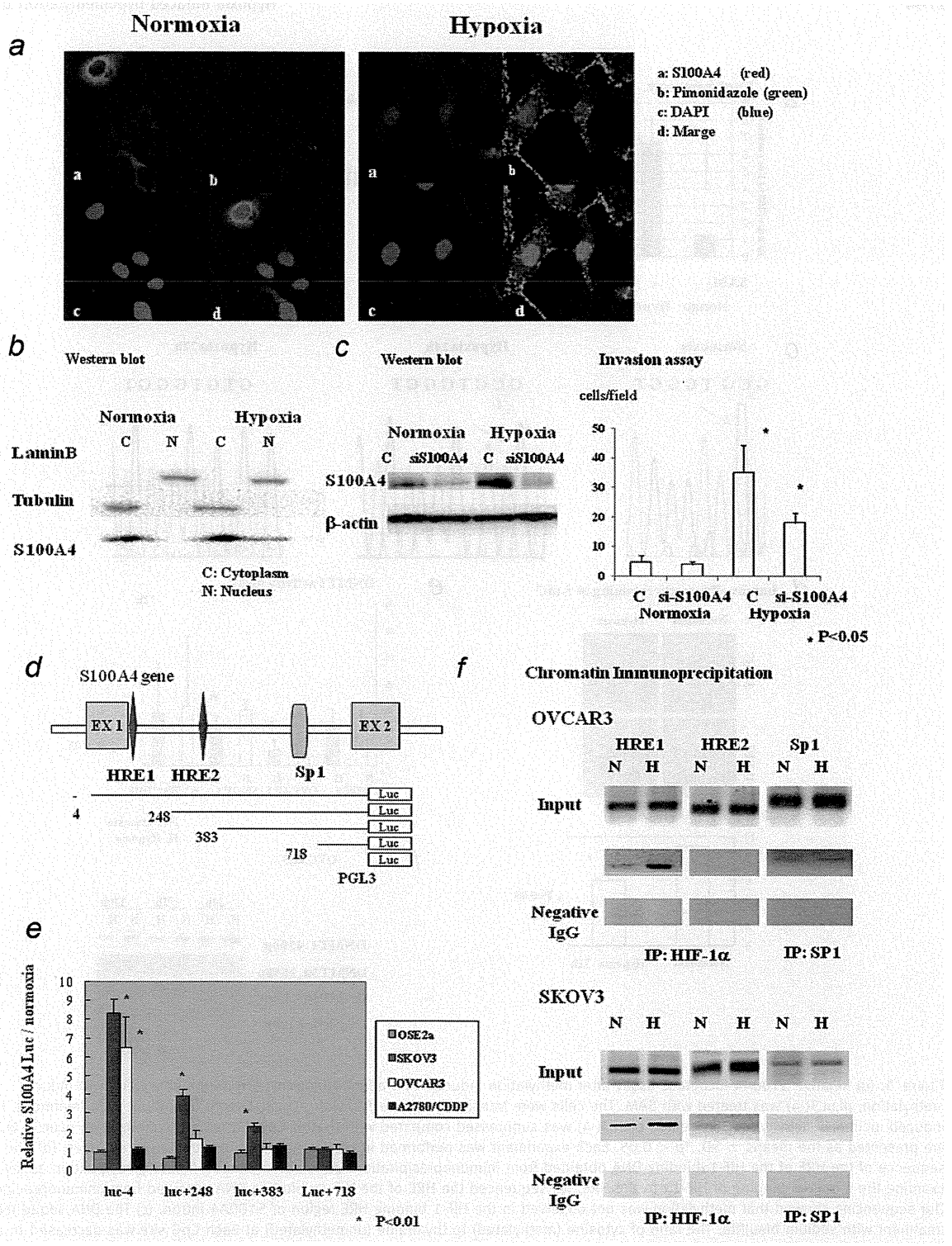

Figure 4. (*a*) Immunofluorescent analysis of the subcellular localization of S100A4 under hypoxia in SKOV3 cells. The nuclear expression of S100A4 was observed under hypoxia, whereas S100A4 expression was observed in the cytoplasm of SKOV3 cells under normoxia. a: S100A4 (red), b: hypoxic marker, Pimonidazole (green), c: DAPI (blue), d: merged. (*b*) Western blot analysis of the cytoplasmic and nuclear fractions. Hypoxia induced nuclear S100A4 expression in SKOV3 cells. N: nuclear fraction, C: cytoplasmic fraction. (*c*) Effects of S100A4 siRNA on the invasive activity of A2780/CDDP cells. The expression of S100A4 after transfection with S100A4 siRNA was analyzed by Western blotting. S100A4 siRNA inhibits the induction of S100A4 expression under hypoxia.100A4 siRNA inhibited the invasiveness induced by hypoxia. Values represent the mean ± SD of three independent experiments. *$p < 0.05$. (*d*) Identification of the HIF-1α response element-binding site in the first intron of the S100A4 gene. (*e*) Luciferase assay in A2780/CDDP, SKOV3, OVCAR3 and OSE2a cells. Values are presented as the means ± SD. *$p < 0.05$. (*f*) Chromatin immunoprecipitation assay (ChIP). HIF-1α bind to HRE1 and HRE2 under hypoxia in SKOV3 cells. Increased HIF-1α. DNA binding to the HRE1 of the S100A4 intron was detected in OVCAR3 cells.

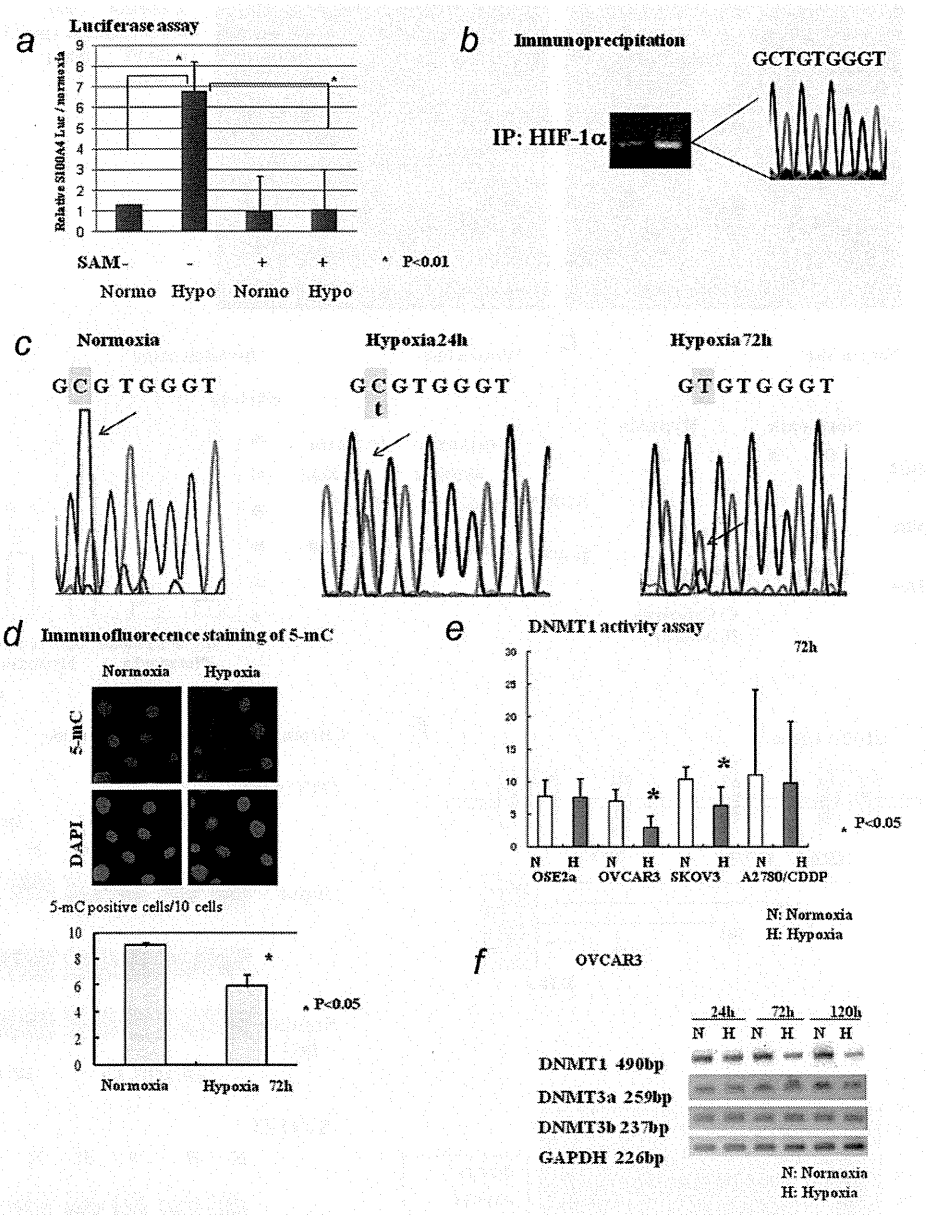

Figure 5. (*a*) Relative S100A4 luciferase assay after methylation induced by s-adenosyl-[methyl-3H] methionine (SAM). To induce methylation, pLuc3(-4) was treated with SAM. The cells were transiently transfected with pLuc3(-4) with or without SAM treatment. Hypoxia-induced luciferase activity of SAM-treated pLuc3(-4) was suppressed compared with that of SAM-untreated unmethylated pLuc3(-4). Values are presented as the means ± SD. $*p < 0.05$. Each experiment was performed in triplicate wells and repeated three times. (*b*) The sequence of the HRE of the HIF-1αbinding DNA obtained from immunoprecipitation. Bands of chromatin immunoprecipitation assay. To examine the impaired binding of HIF-1α to the HRE, we sequenced the HRE of the HIF-1α binding DNA obtained from immunoprecipitation. Our sequencing showed that methylation was not observed in the HIF-1 binding HRE region of S100A4 intron. (*c*) The DNA sequence after treatment with sodium bisulfite. The ratio of cytosine (methylated) to thymidine (unmethylated) at each CpG site was decreased in a time-dependent manner. (*d*) Immunofluorescent staining of 5methyl-cytosine (5-mC). The number of 5-mc-positive cells was significantly decreased under hypoxia. The number of 5-mc-positive cells/10cells was evaluated in ten arbitrary fields. Each experiment was performed in triplicate wells and repeated three times. Upper panel: 5-mC staining (green), Lower panel: Nuclei were counterstained with DAPI (blue). $*p < 0.05$. (*e*) Enzyme assay for DNMT. Reduced DNMT activity after being exposed to hypoxia was observed in OVCAR3 and SKOV3 cell lines. Values are presented as the means ± SD. (*f*) RT-PCR analysis of DNMT1, DNMT3A and DNMT3B. The mRNA expression of the maintenance methyltransferase DNMT1 was decreased under hypoxia in OVCAR3 cells. In contrast, there were no significant changes in the mRNA expression of the *de novo* methyltransferases DNMT3A and DNMT3B.

an important biological marker and a molecular target for ovarian cancer treatment.

Discussion

We previously reported that S100A4 expression was upregulated in ovarian carcinomas and that the nuclear expression of S100A4 was an independent prognostic factor in patients with ovarian cancer.[15] Therefore, in this study, we examined the mechanisms of the upregulation of S100A4 expression in ovarian carcinoma cells, with particular attention paid to the effects of hypoxia. Our experiments showed that the expression levels of S100A4 were correlated with the invasiveness of ovarian carcinoma cells *in vitro* and *in vivo*. In addition, the upregulation of S100A4 expression was associated with the hypomethylation of CpG sites in the first intron of S100A4 in ovarian carcinoma cell lines and tissues. Our findings suggest that DNA hypomethylation is an important mechanism for regulating S100A4 expression in ovarian cancer cells and were compatible with those of studies of other malignant tumors, such as pancreatic, prostate, lymphoma and endometrial carcinoma cells.[16–20] In contrast, Rehman *et al.*[18] reported that intronic CpG methylation does not affect S100A4 expression in blood cells. Thus, whether the increased S100A4 expression is a consequence of gene hypomethylation depends on the cell type.[38] Our findings indicated that the upregulation of S100A4 plays an important role in the acquisition of aggressive characteristics in ovarian carcinomas *via* epigenetic changes.

We then found that hypoxia upregulated S100A4 expression in ovarian cancer cells. The upregulated expression of S100A4 induced under hypoxia resulted in increased invasiveness in SKOV3 cells, which was inhibited by specific siRNA against S100A4. This is the first report to show that the increased invasiveness observed under hypoxia is associated with the induction of S100A4 expression. However, the inhibition of hypoxia-induced invasiveness by specific S100A4 siRNA was not complete; therefore, it might also be caused by other genes that are induced by hypoxia, such as Snail, CXCR4 and lysyl oxidase.[5] The human S100A4 gene has two HRE in its first intron. Our luciferase analysis showed that the sequence of the HRE is important for inducing S100A4 transcriptional activity under hypoxia, and a CHIP assay showed that HIF-1α binds directly to an HRE in intron 1 of the S100A4 gene. Moreover, the suppression of HIF-1α reduced the transcriptional induction of S100A4 under hypoxia. Consistent with our results, Liao *et al.* suggested that the conditional induction of HIF-1α protein induced the expression of several genes, including S100A4 in a leukemic U937T-cell line, using differential gel electrophoresis.[39] Recently, Zhang *et al.*[40] have also reported that hypoxia induced the nuclear expression of S100A4 in gastric cancer cell line BRC823. They showed that HIF-1α binds to HRE2; however, they did not analyze the binding of HIF-1α and HRE1. Taken together, these findings provide evidence for the interaction of HIF-1α and S100A4 under hypoxia.

Moreover, our findings indicate that the methylation status of HRE is important for HIF-1α binding. We found that the HIF-1 binding HRE was methylation free. Similarly, Wenger *et al.*[41] demonstrated that erythropoietin gene expression is dependent on a CpG methylation-free HRE. The increased expression of Class III beta-tubulin under hypoxia is also associated with the methylation status of CpG.[42] Methylated CpG might interfere with the binding of transcription factors through direct steric changes and/or the binding of repressor proteins. These findings suggest that the adaptation to hypoxia is mediated through a coordinated transcriptional response and epigenetic changes. This is the first report to show that the degree of CpG methylation might play a role in the HIF-induced expression of S100A4.

Interestingly, the methylation level of CpG sites was altered under hypoxia. The ratio of cytosine (methylated) to thymidine (unmethylated) at the CpG site was decreased under hypoxia in a time-dependent manner. We found that the activity of DNMT in ovarian cancer cells was also decreased under hypoxia. Shahrzad *et al.*[43] have also demonstrated that hypoxia regulates DNA demethylases and helps to maintain epigenetic homeostasis under hypoxic conditions. Although the role of DNMT under hypoxia in malignant tumors is disputed,[44–46] these results suggest that hypoxic microenvironments affect DNMT activity and induce DNA hypomethylation, leading to an inappropriate reawakening of gene expression. Our findings suggested the possible epigenetic mechanism of the upregulation of S100A4 expression during ovarian cancer progression (Supporting Information Fig. 5). Hypomethylation of the first intron in S100A4 gene is the first step in the upregulation of S100A4. The second step is that hypoxia-induced HIF-1 binds to hypomethylated HRE; however, the biological mechanism of the induction of the *in vivo* hypomethylation of S100A4 has not been fully characterized. Therefore, the epigenetic alterations in the S100A4 gene induced by microenvironmental conditions require further investigation.

Our previous study showed that the nuclear expression of S100A4 was an independent prognostic factor in patients with ovarian cancer.[15] In addition, this study showed that the nuclear expression of S100A4 in combination with nuclear HIF-1α protein is a marker of poor prognosis. Accordingly, the presence of hypoxic conditions might upregulate S100A4 expression, producing an unfavorable prognosis. Although S100A4 was first identified as a cytoplasmic protein, its translocation between the cytoplasm and the nucleus has been reported in human cells.[47,48] The nuclear expression of S100A4 has been reported to be implicated in the regulation of gene transcription either through direct DNA binding or through its interaction with other DNA-binding proteins.[48,49] Our findings suggest that the nuclear expression of S100A4 combined with HIF-1α is an important biological marker and could be a molecular target for ovarian cancer treatment.

This study showed that the upregulation of S100A4 expression was associated with hypomethylation, along with

increased malignancy during ovarian cancer progression. We also found that exposure to hypoxia increased the hypomethylation of the first intron of S100A4 and increased the binding of HIF-1α in ovarian cancer cell lines. These results indicate that hypoxia-induced hypomethylation plays an important role in gene overexpression during tumor progression.

Acknowledgements

The authors extend special thanks to Fumi Tsunoda (Department of Obstetrics and Gynecology, Shinshu University) for providing technical assistance. This work was supported in part by Grants-in-Aid for Scientific Research to A.H. (No. 1859182), N.K. (20591942) and to I.K. (No. 19390426) from the Ministry of Education, Science and Culture of Japan.

References

1. Joyce JA. Therapeutic targeting of the tumor microenvironment. *Cancer Cell* 2005;7:513–20.
2. Semenza GL. Defining the role of hypoxia-inducible factor 1 in cancer biology and therapeutics. *Oncogene* 2010;29:625–34. (Epub 2009 Nov 30).
3. Harris AL. Hypoxia—a key regulatory factor in tumour growth. *Nat Rev Cancer* 2002;2:38–47.
4. Graeber TG, Osmanian C, Jacks T, Housman DE, Koch CJ, Lowe SW, Giaccia AJ. Hypoxia-mediated selection of cells with diminished apoptotic potential in solid tumours. *Nature* 1996;379:88–91.
5. Rankin EB, Giaccia AJ. The role of hypoxia-inducible factors in tumorigenesis. *Cell Death Differ* 2008;15:678–85.
6. Semenza GL. Regulation of mammalian O2 homeostasis by hypoxia-inducible factor 1. *Annu Rev Cell Dev Biol* 1999;15:551–78.
7. Imai T, Horiuchi A, Wang C, Oka K, Ohira S, Nikaido T, Konishi I. Hypoxia attenuates the expression of E-cadherin via up-regulation of SNAIL in ovarian carcinoma cells. *Am J Pathol* 2003;163:1437–47.
8. Horiuchi A, Imai T, Shimizu M, Oka K, Wang C, Nikaido T, Konishi I. Hypoxia-induced changes in the expression of VEGF, HIF-1 alpha and cell cycle-related molecules in ovarian cancer cells. *Anticancer Res* 2002;22:2697–702.
9. Osada R, Horiuchi A, Kikuchi N, Yoshida J, Hayashi A, Ota M, Katsuyama Y, Melillo G, Konishi I. Expression of hypoxia-inducible factor 1alpha, hypoxia-inducible factor 2alpha, and von Hippel-Lindau protein in epithelial ovarian neoplasms and allelic loss of von Hippel-Lindau gene: nuclear expression of hypoxia-inducible factor 1alpha is an independent prognostic factor in ovarian carcinoma. *Hum Pathol* 2007;38:1310–20.
10. Donato R. S100: a multigenic family of calcium-modulated proteins of the EF-hand type with intracellular and extracellular functional roles. *Int J Biochem Cell Biol* 2001;33:637–68.
11. Boye K, Maelandsmo GM. S100A4 and metastasis: a small actor playing many roles. *Am J Pathol* 2010;176:528–35.
12. Hiratsuka S, Nakamura K, Iwai S, Murakami M, Itoh T, Kijima H, Shipley JM, Senior RM, Shibuya M. MMP9 induction by vascular endothelial growth factor receptor-1 is involved in lung-specific metastasis. *Cancer Cell* 2002;2:289–300.
13. Hiratsuka S, Watanabe A, Aburatani H, Maru Y. Tumour-mediated upregulation of chemoattractants and recruitment of myeloid cells predetermines lung metastasis. *Nat Cell Biol* 2006;8:1369–75.
14. Harris MA, Yang H, Low BE, Mukherjee J, Guha A, Bronson RT, Shultz LD, Israel MA, Yun K. Cancer stem cells are enriched in the side population cells in a mouse model of glioma. *Cancer Res* 2008;68:10051–9.
15. Kikuchi N, Horiuchi A, Osada R, Imai T, Wang C, Chen X, Konishi I. Nuclear expression of S100A4 is associated with aggressive behavior of epithelial ovarian carcinoma: an important autocrine/paracrine factor in tumor progression. *Cancer Sci* 2006;97:1061–9.
16. Sato N, Maitra A, Fukushima N, van Heek NT, Matsubayashi H, Iacobuzio-Donahue CA, Rosty C, Goggins M. Frequent hypomethylation of multiple genes overexpressed in pancreatic ductal adenocarcinoma. *Cancer Res* 2003;63:4158–66.
17. Xie R, Loose DS, Shipley GL, Xie S, Bassett RL, Jr. Broaddus RR. Hypomethylation-induced expression of S100A4 in endometrial carcinoma. *Mod Pathol* 2007;20:1045–54.
18. Rehman I, Goodarzi A, Cross SS, Leiblich A, Catto JW, Phillips JT, Hamdy FC. DNA methylation and immunohistochemical analysis of the S100A4 calcium binding protein in human prostate cancer. *Prostate* 2007;67:341–7.
19. Rosty C, Ueki T, Argani P, Jansen M, Yeo CJ, Cameron JL, Hruban RH, Goggins M. Overexpression of S100A4 in pancreatic ductal adenocarcinomas is associated with poor differentiation and DNA hypomethylation. *Am J Pathol* 2002;160:45–50.
20. Tulchinsky E, Grigorian M, Tkatch T, Georgiev G, Lukanidin E. Transcriptional regulation of the mts1 gene in human lymphoma cells: the role of DNA-methylation. *Biochim Biophys Acta* 1995;1261:243–8.
21. Lujambio A, Esteller M. How epigenetics can explain human metastasis: a new role for microRNAs. *Cell Cycle* 2009;8:377–82.
22. Goelz SE, Vogelstein B, Hamilton SR, Feinberg AP. Hypomethylation of DNA from benign and malignant human colon neoplasms. *Science* 1985;228:187–90.
23. Feinberg AP, Vogelstein B. Hypomethylation distinguishes genes of some human cancers from their normal counterparts. *Nature* 1983;301:89–92.
24. Jang SJ, Soria JC, Wang L, Hassan KA, Morice RC, Walsh GL, Hong WK, Mao L. Activation of melanoma antigen tumor antigens occurs early in lung carcinogenesis. *Cancer Res* 2001;61:7959–63.
25. Ehrlich M. DNA methylation in cancer: too much, but also too little. *Oncogene* 2002;21:5400–13.
26. Yanagawa N, Tamura G, Honda T, Endoh M, Nishizuka S, Motoyama T. Demethylation of the synuclein gamma gene CpG island in primary gastric cancers and gastric cancer cell lines. *Clin Cancer Res* 2004;10:2447–51.
27. Kwapiszewska G, Wilhelm J, Wolff S, Laumanns I, Koenig IR, Ziegler A, Seeger W, Bohle RM, Weissmann N, Fink L. Expression profiling of laser-microdissected intrapulmonary arteries in hypoxia-induced pulmonary hypertension. *Respir Res* 2005;6:109.
28. Tsuruo T, Hamilton TC, Louie KG, Behrens BC, Young RC, Ozols RF. Collateral susceptibility of adriamycin-, melphalan- and cisplatin-resistant human ovarian tumor cells to bleomycin. *Jpn J Cancer Res* 1986;77:941–5.
29. Nitta M, Katabuchi H, Ohtake H, Tashiro H, Yamaizumi M, Okamura H. Characterization and tumorigenicity of human ovarian surface epithelial cells immortalized by SV40 large T antigen. *Gynecol Oncol* 2001;81:10–7.
30. Horiuchi A, Imai T, Wang C, Ohira S, Feng Y, Nikaido T, Konishi I. Up-regulation of small GTPases, RhoA and RhoC, is associated with tumor progression in ovarian carcinoma. *Lab Invest* 2003;83:861–70.
31. Horiuchi A, Nikaido T, Taniguchi S, Fujii S. Possible role of calponin h1 as a tumor suppressor in human uterine leiomyosarcoma. *J Natl Cancer Inst* 1999;91:790–6.
32. Horiuchi A, Nikaido T, Ito K, Zhai Y, Orii A, Taniguchi S, Toki T, Fujii S. Reduced expression of calponin h1 in leiomyosarcoma of the uterus. *Lab Invest* 1998;78:839–46.
33. Wang C, Horiuchi A, Imai T, Ohira S, Itoh K, Nikaido T, Katsuyama Y, Konishi I. Expression of BRCA1 protein in benign, borderline, and malignant epithelial ovarian neoplasms and its relationship to methylation and allelic loss of the BRCA1 gene. *J Pathol* 2004;202:215–23.
34. Grzendowski M, Wolter M, Riemenschneider MJ, Knobbe CB, Schlegel U, Meyer HE, Reifenberger G, Stuhler K. Differential proteome analysis of human gliomas stratified for loss of heterozygosity on chromosomal arms 1p and 19q. *Neuro Oncol* 2010;12:243–56.
35. Wenger RH, Gassmann M. Oxygen(es) and the hypoxia-inducible factor-1. *Biol Chem* 1997;378:609–16.
36. Wilkins JF. Genomic imprinting and methylation: epigenetic canalization and conflict. *Trends Genet* 2005;21:356–65.
37. Okano M, Xie S, Li E. Dnmt2 is not required for de novo and maintenance methylation of viral DNA in embryonic stem cells. *Nucleic Acids Res* 1998;26:2536–40.
38. Dokun OY, Florl AR, Seifert HH, Wolff I, Schulz WA. Relationship of SNCG, S100A4, S100A9 and LCN2 gene expression and DNA methylation in bladder cancer. *Int J Cancer* 2008;123:2798–807.
39. Liao SH, Zhao XY, Han YH, Zhang J, Wang LS, Xia L, Zhao KW, Zheng Y, Guo M, Chen GQ. Proteomics-based identification of two novel direct targets of hypoxia-inducible factor-1 and their potential roles in migration/invasion of cancer cells. *Proteomics* 2009;9:3901–12.

40. Zhang R, Fu H, Chen D, Hua J, Hu Y, Sun K, Sun X. Subcellular distribution of S100A4 and its transcriptional regulation under hypoxic conditions in gastric cancer cell line BGC823. *Cancer Sci* 2010;101:1141–6.
41. Wenger RH, Kvietikova I, Rolfs A, Camenisch G, Gassmann M. Oxygen-regulated erythropoietin gene expression is dependent on a CpG methylation-free hypoxia-inducible factor-1 DNA-binding site. *Eur J Biochem* 1998; 253:771–7.
42. Raspaglio G, Filippetti F, Prislei S, Penci R, De Maria I, Cicchillitti L, Mozzetti S, Scambia G, Ferlini C. Hypoxia induces class III beta-tubulin gene expression by HIF-1alpha binding to its 3′ flanking region. *Gene* 2008;409:100–8.
43. Shahrzad S, Bertrand K, Minhas K, Coomber BL. Induction of DNA hypomethylation by tumor hypoxia. *Epigenetics* 2007;2:119–25.
44. Skowronski K, Dubey S, Rodenhiser D, Coomber B. Ischemia dysregulates DNA methyltransferases and p16INK4a methylation in human colorectal cancer cells. *Epigenetics* 2010;5:547–56.
45. Peng DF, Kanai Y, Sawada M, Ushijima S, Hiraoka N, Kitazawa S, Hirohashi S. DNA methylation of multiple tumor-related genes in association with overexpression of DNA methyltransferase 1 (DNMT1) during multistage carcinogenesis of the pancreas. *Carcinogenesis* 2006;27:1160–8.
46. Sato M, Horio Y, Sekido Y, Minna JD, Shimokata K, Hasegawa Y. The expression of DNA methyltransferases and methyl-CpG-binding proteins is not associated with the methylation status of p14(ARF), p16(INK4a) and RASSF1A in human lung cancer cell lines. *Oncogene* 2002;21: 4822–9.
47. Hsieh HL, Schafer BW, Weigle B, Heizmann CW. S100 protein translocation in response to extracellular S100 is mediated by receptor for advanced glycation endproducts in human endothelial cells. *Biochem Biophys Res Commun* 2004;316:949–59.
48. Flatmark K, Pedersen KB, Nesland JM, Rasmussen H, Aamodt G, Mikalsen SO, Bjornland K, Fodstad O, Maelandsmo GM. Nuclear localization of the metastasis-related protein S100A4 correlates with tumour stage in colorectal cancer. *J Pathol* 2003;200: 589–95.
49. Saleem M, Kweon MH, Johnson JJ, Adhami VM, Elcheva I, Khan N, Bin Hafeez B, Bhat KM, Sarfaraz S, Reagan-Shaw S, Spiegelman VS, Setaluri V, et al. S100A4 accelerates tumorigenesis and invasion of human prostate cancer through the transcriptional regulation of matrix metalloproteinase 9. *Proc Natl Acad Sci USA* 2006;103:14825–30.

European Journal of Immunology

Differential effects of inhibition of bone morphogenic protein (BMP) signalling on T-cell activation and differentiation

Yumiko Yoshioka[*1,2], *Masahiro Ono*[2,3,4,*], *Motonao Osaki*[2], *Ikuo Konishi*[1] *and Shimon Sakaguchi*[2,3]

[1] Department of Gynecology and Obstetrics, Graduate School of Medicine, Kyoto University, Kyoto, Japan
[2] Department of Experimental Pathology, Institute for Frontier Medical Sciences, Kyoto University, Kyoto, Japan
[3] WPI Immunology Frontier Research Center, Osaka University, Suita, Japan
[4] Immunobiology Unit, Institute of Child Health, University College London, London

Bone morphogenetic proteins (BMPs) are involved in patterning and cellular fate in various organs including the thymus. However, the redundancy of BMPs and their receptors have made it difficult to analyse their physiological roles. Here, we investigated the role of BMP signalling in peripheral $CD4^+$ T cells by analysing the effects of an inhibitor of BMP signalling, dorsomorphin. Dorsomorphin suppressed phosphorylation of SMAD1/5/8, suggesting that BMP signalling naturally occurs in T cells. At high doses, dorsomorphin suppressed proliferation of T cells in a dose-dependent manner, inducing G1 arrest. Also, dorsomorphin suppressed Th17 and induced Treg-cell differentiation, while preserving Th2 differentiation. Dorsomorphin efficiently suppressed IL-2 production even at low doses in mouse $CD4^+$ T cells, suggesting that the BMP-Smad signalling physiologically regulates IL-2 transcription in these cells. In addition, recombinant BMP2 induced a dose-dependent multiphasic pattern of IL-2 production, while Noggin suppressed IL-2 production at higher doses in Jurkat cells. Notably, BMP signalling controlled the phosphorylation of RUNX1, revealing the molecular nature of its effect. Collectively, we describe multiple effects of dorsomorphin and Noggin on T-cell activation and differentiation, demonstrating a physiological role for BMP signalling in these processes.

Key words: Bone morphogenic protein · $CD4^+$ T cells · IL-2 · Morphogen · T-cell activation

Supporting Information available online

Introduction

T cells are continuously generated in the thymus, and differentiate into more mature T cells in the periphery throughout life. Thus, not surprisingly, many mechanisms involved in embryogenesis are used in thymocytes and T cells. Bone morphogenetic proteins (BMPs) have important roles in embryogenesis and organogenesis of various tissues including the development of the thymus [1]. It has been reported that BMP2 and BMP4 and their extracellular inhibitors, Noggin and Chordin, are expressed in the thymus, and that BMP4 inhibits the transition from $CD4^-CD8^-$ double negative (DN) to $CD4^+CD8^+$ double positive (DP) and

Correspondence: Dr. Masahiro Ono
e-mail: m.ono@ucl.ac.uk

*These authors contributed equally to this work.

arrests cells at the $CD25^{-}CD44^{+}$ and $CD25^{+}CD44^{-}$ DN stages [2, 3]. On the other hand, inhibition of BMP2/4 signalling by Noggin promotes and accelerates thymocyte differentiation, increasing the proportions of $CD44^{-}CD25^{-}$ DN thymocytes and DP thymocytes [2, 3]. In the periphery, the developmental or differentiation processes of T cells are studied as "T-cell activation and differentiation". Thus, the roles of BMP can be reasonably addressed in some aspects of these processes. Recently, BMPs have been suggested to have some roles in peripheral T-cell proliferation, although their physiological relevance and mechanisms are still unclear [4].

BMPs are made up of more than 20 distinct BMP subunits, and belong to the larger transforming growth factor-beta (TGF-β ligand family [5]. BMP forms heterodimers or homodimers, which make heterotetrameric complexes with type I and II BMP receptors (BMPRs), and transduce signals via the complex. BMP ligands are recognized by the pairs of type II BMPR or Activin type II receptor (ActRIIa and ActRIIb) with various BMP type I receptors (ALK1, ALK2, ALK3, and ALK6). When engaged by ligand, type II BMPR phosphorylates type I BMPR, which triggers phosphorylation of BMP-responsive receptor-regulated SMADs (R-SMADs, namely, SMAD1, SMAD5 and SMAD8). R-SMADs form a complex with common-partner SMADs (Co- SMADs: SMAD4) and translocate into the nucleus, where the complex regulates the transcription of its target genes [6]. It is known that the SMAD complex interacts with the transcription factor RUNX2, which is a major target of BMP signalling for the differentiation of osteoblasts [7]. In hematopoietic stem cells, BMP4/SMAD signalling is reported to regulate RUNX1 activity [8]. Preceding studies indicate that BMP activates not only the SMAD pathway but also other pathways such as mitogen-activated protein kinase (MAPK) family of molecules including ERK1/2 and p38 [9].

Considering the number of combinations of BMP ligands and receptors, we attempted to address the possible roles of BMP signalling in T-cell activation and differentiation by inhibiting a wide range of BMP signalling using a small molecule inhibitor of type I BMPRs, dorsomorphin (DM) [10]. In this study, we analysed the perturbation effects of DM in $CD4^{+}$ T cells, in order to identify functional consequences of inhibition of BMP signalling in T cells. We found that DM differentially affected the processes of T-cell activation in a unique manner. Presumably, some, if not all, of the mechanisms affected by DM-treatment should include those truly regulated by BMP signalling in T cells.

Results

DM inhibits BMP-SMAD1/5/8 signalling in Jurkat cells

We investigated the role of the BMP signalling pathway by analysing the effects of its inhibitor. A small molecule compound, DM, is reported to selectively decrease the level of SMAD1/5/8 phosphorylation by inhibiting the kinase activity of BMP type I receptor [11]. We confirmed this specific effect of DM on SMAD1/5/8 phosphorylation in Jurkat cells (Fig. 1). DM decreased the level of phosphorylation of SMAD1/5/8 (p-SMAD1/5/8) in both BMP2-treated and non-treated Jurkat cells (Fig. 1A and B). Although the signal/noise ratio of the detection of p-SMAD1/5/8 by western blot using Jurkat were not large, DM clearly inhibited phosphorylation of SMAD1/5/8 in Jurkat cells in a dose-dependent manner, and the half maximal inhibitory concentration (IC_{50}) was ~0.31 μM, which was comparable to the preceding study (Fig. 1C and D, [11]). On the other hand, dorsomophin did not inhibit phosphorylation of SMAD2, which mediates TGF-β signalling (Fig. 1C and D). In addition, BMP2 increased phosphorylation of Smad1/5/8 in mouse $CD4^{+}$ T cells, whereas DM inhibited it in both BMP2-treated and non-treated T cells (Supporting Information Fig. 1). Thus, DM is a specific inhibitor of BMP-SMAD signalling in T cells, as the previous report showed using pulmonary artery smooth muscle cells [11].

DM inhibits T-cell proliferation

Next, we addressed functional consequences of the inhibition of BMP-SMAD signalling by DM. Jurkat or mouse $CD4^{+}$ T cells were cultured with titrated doses of DM (0.1–20 μM) under stimulation with anti-CD3 and -CD28 antibodies for 60 h. Thymidine incorporation assay revealed that DM suppressed the proliferation of both Jurkat and mouse $CD4^{+}$ T cells in a dose-dependent manner (IC_{50} ~ 2.43 μM, 1.40 μM, respectively, Fig. 2A and B). As expected from this result, DM inhibited cell division of mouse $CD4^{+}$ $CD25^{-}$ naïve T cells by the carboxyfluorescein diacetate succinimidyl ester (CFSE) dilution assay. In the CFSE dilution assay, almost all cells were dead when the concentration of DM was higher than 10 μM (Supporting Information Fig. 2A), presumably because of the synergistic toxicities of CFSE and DM (Fig. 3). DM clearly inhibited cell division by the CFSE dilution assay at the concentrations above 1 μM (Fig. 2C), which was compatible with the results of thymidine incorporation. The Proliferation Index (the average number of cell divisions that a cell in the original population has undergone) showed a dose-dependent inhibition of cell division, while mean fluorescence intensity (MFI) and Division Index (the average number of cell divisions that the responding cells underwent) showed a mild increase of cell division at the low concentration of DM (Fig. 2C). This result suggests that low concentrations of DM can mildly promote the proliferation of dividing T cells. This issue will be addressed below.

DM induces G0/G1 arrest in T cells

In order to analyse more precisely how DM suppresses the proliferation of T cells, we performed cell cycle analysis of DM-treated cells. Jurkat cells were stimulated by anti-CD3 and -CD28 antibodies with DM or DMSO as a control. Cultured cells were analysed 2 days after stimulation by flow cytometry using bromodeoxyuridine (BrdU) label and 7-Amino-actinomycin D (7AAD) staining. The percentages of sub-G1 positive cells were comparable between control and DM-treated cells (6.8 versus

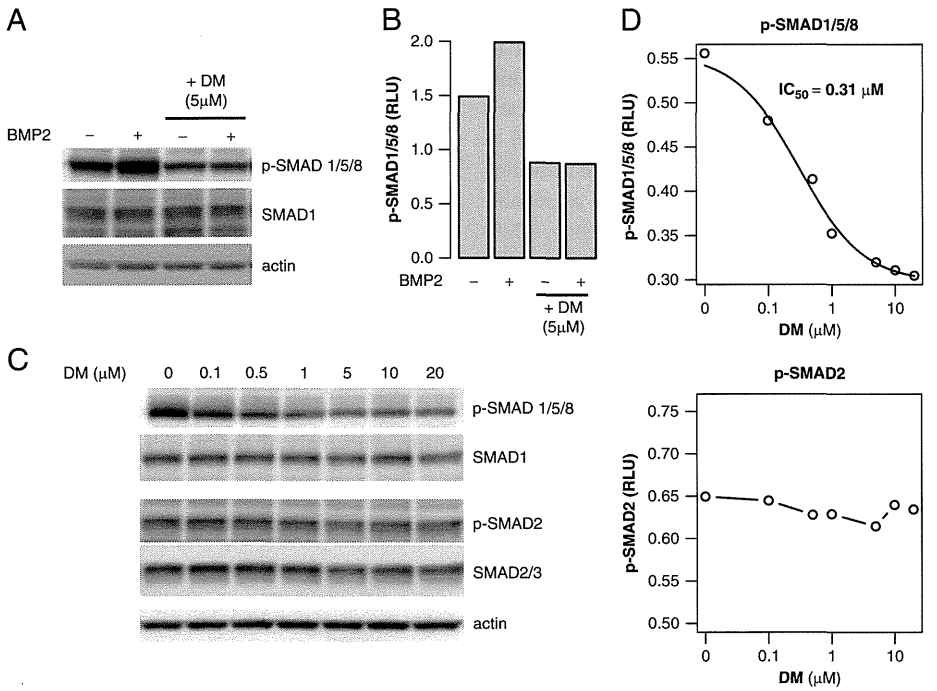

Figure 1. The effect of DM on the phosphorylation of SMAD1/5/8. (A) Western blotting of phosphorylated SMAD1/5/8 (p-SMAD1/5/8) in Jurkat cells cultured with or without BMP2 in the presence of DM or DMSO as a control. Cells were cultured for 30 min with indicated conditions and stimulated with anti-CD3 and -CD28 antibodies for 1 h. (B) Densitometric analysis of p-SMAD1/5/8 in (A). Intensities of p-SMAD1/5/8 were normalised to those of total SMAD1. (C) Western blotting of p-SMAD1/5/8, SMAD1, p-SMAD2, and SMAD2/3 in Jurkat cells cultured with titrated doses of DM. (D) Densitometric analysis of p-SMAD1/5/8 and p-SMAD2 in (C). Intensities of p-SMAD1/5/8 (left) and p-SMAD2 (right) were normalized to those of total SMAD1 and SMAD2/3 respectively. Data were regressed to a four-parameter log-logistic function in p-SMAD1/5/8. Actin was used for a loading control (A, C). All figures are representative of three independent experiments.

7.2%), suggesting that obvious apoptosis or necrosis did not occur in DM-treated cells at this time point (Fig. 3A). The percentage of G0/G1 cells was increased in DM-treated cells compared with control cells (67.5 versus 57.3%, Fig. 3A). On the other hand, the percentage of S-phase cells was decreased in DM-treated cells (9.3 versus 17.6%, Fig. 3A).

The cyclin-dependent kinase inhibitor $p27^{kip1}$ is known to inhibit CDK2 and the G1-S transition, and previous studies indicate that the protein level of $p27^{kip1}$ is increased in anergic T cells [12]. Western blotting of lysates from Jurkat cells cultured with DM showed that DM accumulated $p27^{kip1}$ in Jurkat cells (Fig. 3B). These results indicate that DM inhibits the G1-S transition.

Flow cytometric evaluation of apoptosis using Annexin V and 7AAD staining confirmed that DM-treated, mouse $CD4^+CD25^-$ naïve T cells were not obviously apoptotic (Fig. 3C and D). In the later days of cell culture, control cells were more apoptotic (Fig. 3C and D), suggesting that activation-induced cell death occurs more in control cells.

CD25 expression upon TCR stimulation is attenuated by DM

The results of flow cytometric evaluation of apoptosis suggested that T-cell activation is suppressed in DM-treated T cells. To address this issue, we analysed the flow cytometric features of activated T cells including the expression of the activation marker of T cells, CD25 (IL-2 receptor α chain), upon stimulation. $CD4^+$ $CD25^-$ T cells were stimulated by anti-CD3 and CD28 with DM (5 μM) or DMSO as a control. Both DM-treated cells and control cells increased FSC and SSC (Fig. 4). CD25 expression occurred both in DM-treated and control cells on both days 1 and 4, although the intensities of CD25 expression were lower in DM-treated T cells (MFI: d1, 600 versus 819; d4, 657 versus 1107, Fig. 4). These results suggest that T-cell activation occurs but is partially suppressed by DM.

DM differentially affects helper and regulatory T-cell differentiation in a unique manner

Next, we analysed DM-induced perturbation of differentiation of Th1, Th2, Th17, and induced regulatory T cells (iTreg cells) in vitro. Mouse $CD4^+CD25^-$ naïve T cells were cultured with DM (4 μM) under the Th/Treg polarizing conditions, and their cytokine production and differentiation status were analysed on days 2, 4, and 8 by flow cytometric analysis of intracellular cytokines or Foxp3. DM significantly inhibited the differentiation of Th17 and iTreg cells, while relatively unaffecting the percentages of differentiated Th2 cells at the early stages of cell culture (Fig. 5A

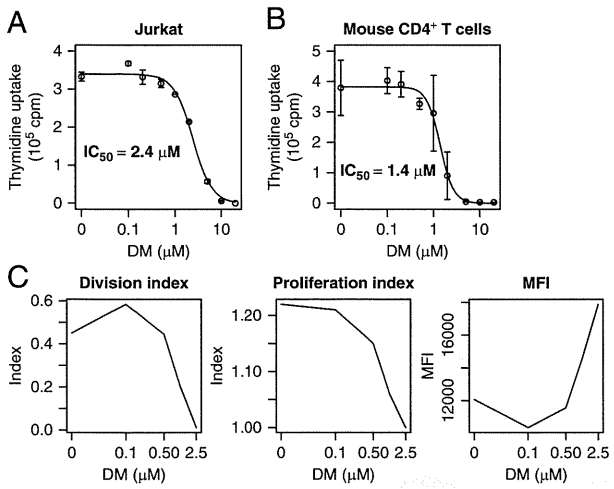

Figure 2. The effects of DM on the proliferation of mouse T cells and Jurkat cells. (A, B) Proliferation of (A) Jurkat or (B) mouse $CD4^+$ T cells cultured with titrated doses of DM was determined by thymidine incorporation. Freshly isolated $CD4^+$ T cells were cultured for 72 h with anti-CD3 and -CD28 antibodies. Data were regressed to a four-parameter log-logistic function. Data are shown as mean ± SD of triplicates. (C) Proliferation of T cells was also measured by CFSE dilution assay. Mouse $CD4^+$ $CD25^-$ naïve T cells were cultured with titrated doses of DM, and stimulated by anti-CD3 antibody with T-cell-depleted splenic APCs. Flow cytometric analysis of cultured cells was performed 48 h after stimulation to analyse the intensity of CFSE. The Division Index (the average number of cell divisions that the responding cells underwent), Proliferation Index (the average number of cell divisions that a cell in the original population has undergone) and mean-fluorescence intensity (MFI) of CFSE-stained T cells are shown. See Supporting Information Fig. 1A for gating strategies and density plots for CFSE dilution. All figures are representative of three independent experiments.

and B). Th17 cell differentiation seemed to be continuously suppressed throughout the culture. Interestingly, exogenous IL-2 did not reverse DM-induced effects (Fig. 5A and B). These results indicate that DM affects not only *IL2* transcription (see below) but also other processes that regulate Th/reg differentiation and are independent of IL-2 signalling.

The expressions of the lineage-specific transcription factors of Th cells were analysed by qPCR. DM markedly suppressed the expression of *Tbx21* and *Rorc*, the lineage-specific transcription factors of Th1 and Th17 cells respectively, but did not suppress the expression of *Gata3*, the lineage-specific transcription factor of Th2 cells (Fig. 5C).

Transcriptomic characteristics of DM-treated T cells

In order to obtain the bigger picture of the effects of DM in T-cell activation, transcriptomic analysis was performed using mouse primary $CD25^-CD4^+$ T cells with either DM (4 μM) or vehicle in the presence or absence of stimulation by anti-CD3 and -CD28 antibodies. A moderated *t*-statistic identified 8259 genes as differentially expressed genes in DM-treated T cells (Supporting Information Fig. 3A). More than a third of the genes that were regulated by stimulation were not significantly regulated by DM (Supporting Information Fig. 3A). In contrast, no differentially expressed genes were identified between DM-treated, unstimulated and stimulated T cells, suggesting that DM-treated cells were hyporesponsive upon activation (Supporting Information Fig. 3A and B). Interestingly, however, the expressions of nearly half of the genes that were significantly regulated by DM were not significantly changed by stimulation only (Supporting Information Fig. 3A). Thus, DM seems to induce some unique and specific effects in T cells independent from the general activation process. To characterise these, we performed a pathway analysis [13]. The mechanisms that were downregulated by DM included TCR signalling pathway, helper T-cell surface molecules, and apoptosis-related mechanisms, which are compatible with findings in Figs. 3 and 4 (Supporting Information Fig. 3C). On the other hand, the mechanisms that were upregulated by DM included IL-6 and p38 MAPK singalling pathways. As expected, the mechanisms that were downregulated by the effects of stimulation considering the effects of DM (statistical interaction between DM and stimulation) included chemokines and cytokines, further confirming the results in Figs. 3 and 6. On the other hand, MAPK signalling pathway was identified in the mechanisms that were upregulated in the interaction of stimulation and DM (Supporting Information Fig. 3D). Assume that p38 MAPK pathway is related to BMP-SMAD pathway [9], the apparent increase in the transcripts that were related to this pathway may be considered as a compensatory feedback mechanism. If we assume this relationship between the inhibition of signalling and the compensatory feedback mechanism in transcripts, the observation that TCR signaling pathway was found in the downregulated mechanisms in DM-treated T cells (Supporting Information Fig. 3C) rather supports that the effects of DM is not a simple consequence of the inhibition of TCR signalling pathway.

A complex effect of DM on IL-2 production of T cells

To further address how DM affects T-cell function, we analysed the perturbation of IL-2 production and T-cell differentiation by DM. We focused on IL-2 production for the following reasons. First, IL-2 production is the crucial mechanism of T-cell activation. Second, *IL2* transcription is known to be regulated by several key transcription factors, one of which is AML1/RUNX1, a well-established downstream target of BMP signalling in hematopoietic lineage cells [8, 14, 15].

We found that DM inhibited IL-2 production of Jurkat and mouse $CD4^+$ T cells in a dose-dependent manner (Fig. 6A). Interestingly, IC_{50} of DM for inhibiting the IL-2 production was smaller in mouse $CD4^+$ T cells (~0.73 μM) than in Jurkat cells (~4.2 μM). Quantitative real-time PCR (qPCR) analysis of IL-2 mRNA revealed that DM markedly decreased *IL2* transcript in Jurkat cells at as early as 3 h after stimulation at the concentration of IC_{50} (Fig. 6B).

Interestingly, the dose–response curve of IL-2 production upon TCR stimulation consistently showed a fluctuation at low

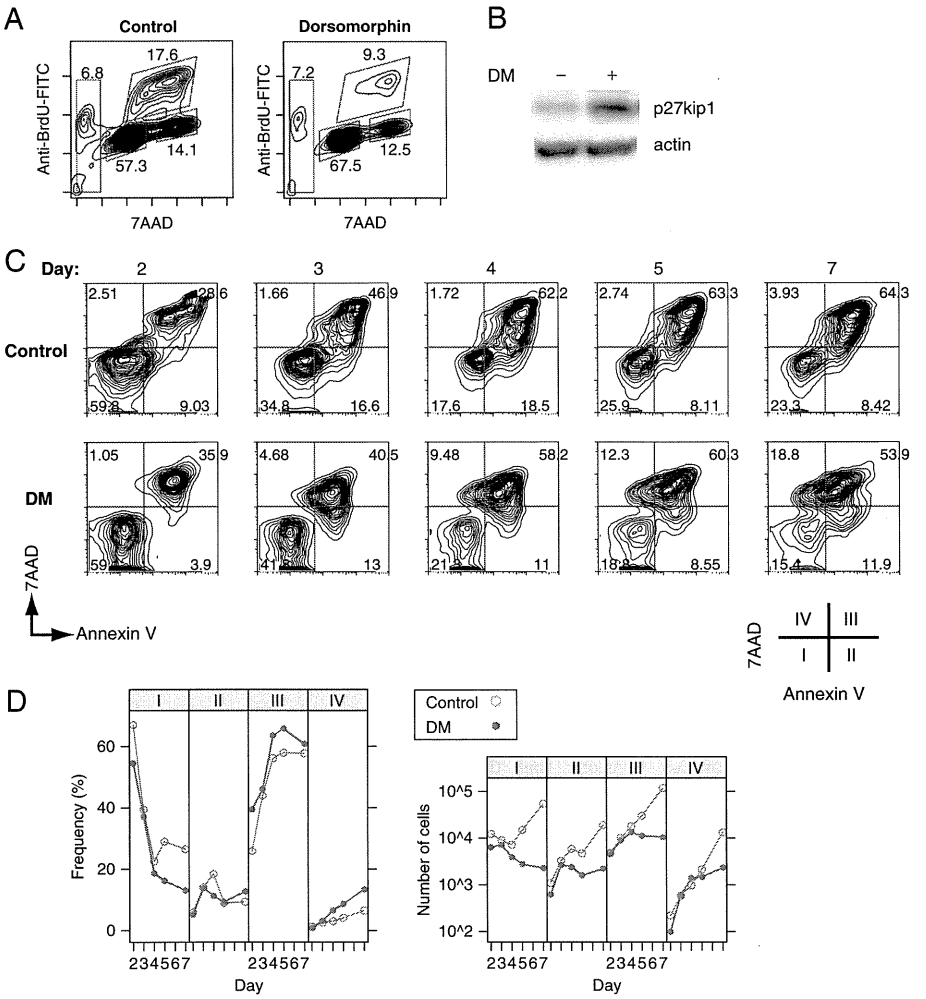

Figure 3. The effects of DM on cell cycle. (A) Jurkat cells were cultured for 2 days with anti-CD3 and -CD28 antibodies with DM (DM, 5 μM) or DMSO as a control, then pulsed with BrdU for last 1 h. Subsequently, cells were fixed, permeabilised, and stained with anti-BrdU and 7AAD. (B) Western blotting analysis of $p27^{kip1}$, cyclin-dependent kinase inhibitor, in DM-treated Jurkat cells. Cells were treated with DM for 30 min, followed by stimulation with anti-CD3 and -CD28 antibodies for 1 h. Actin served as a loading control. (C, D) Analysis of apoptosis in DM-treated T cells by flow cytometry. Freshly isolated $CD4^+CD25^-$ naïve T cells cultured with DM (5 μM), plate bound anti-CD3 and soluble anti-CD28 antibodies for 2–7 days. Cultured cells were fixed and permeabilised, and subsequently stained with AnnexinV and 7AAD. Contour plots in (A) are ungated data. All figures are representative of two independent experiments.

concentrations of DM (0.1–2 μM) in Jurkat cells, and were poorly fit to typical dose–response curves using log-logistic functions in this range, while those at relatively higher concentrations did (Fig. 6A). This wave-like pattern of dose response was also observed in IL-2 production of Jurkat cells cultured with recombinant BMP2 protein (rBMP2, Fig. 6C). Treatment with a fixed concentration of either DM or recombinant Noggin (rNoggin) shifted the multiphasic pattern of IL-2 production by rBMP2 in Jurkat cells (Supporting Information Fig. 4). Treatment with titrated doses of rNoggin showed that there was a significant negative correlation between the dose of rNoggin and IL-2 production ($r = -0.57$, $p<0.001$) by Spearman's correlation coefficient (Fig. 6C). In addition, we have confirmed that knock down of SMAD1 and SMAD5 reduced BMP2-mediated IL-2 production (Fig. 6D). On the other hand, mouse $CD4^+$ T cells were less responsive to rBMP2 and rNoggin, and the correlations between the doses of rNoggin or rBMP2 and IL-2 production were not statistically significant (Fig. 6C). Yet, they showed similar trends to those of Jurkat cells (Fig. 6C). Considering that mouse $CD4^+$ T cells were sensitive to DM in terms of IL-2 production, these results suggest a possibility that the BMP milieu of mouse $CD4^+$ T cells was functionally saturated by a number of BMP ligands. These results collectively suggest that BMP-SMAD signalling regulates *IL2* transcription. The multiphasic effects of DM and rBMP2 suggest that a complex feedback mechanism may exist in BMP-SMAD signalling. Further studies are required to address this point.

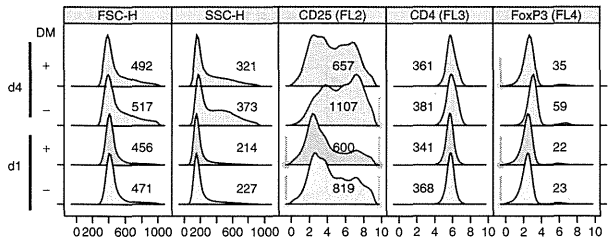

Figure 4. Expression of T-cell activation marker CD25 in DM-treated T cells upon TCR stimulation. Freshly isolated $CD4^+CD25^-$ naïve T cells were cultured with CD3 and -CD28 antibodies with DM (5 μM) or DMSO as a control. Cultured cells were stained with CD25-PE and analysed by flow cytometry on days 1 and 4. These density plots are ungated data. Numbers indicate MFI. Representative results of two independent experiments are shown.

Regulation of phosphorylation of AML1/ RUNX1 by BMP signaling

The results above suggest that BMP signalling modulates RUNX1-mediated *IL2* transcription. As AML/RUNX proteins are reported to be involved in BMP signalling in other tissues such as hematopoitic stem cells [8] and RUNX1 is reported as an important transcription factor for T-cell function including IL-2 production [15], we investigated the molecular mechanism of BMP signalling by analysing RUNX1. The phosphorylated form of RUNX1 with phosphorylation sites including Ser249 is believed to be the activated form of the transcription factor [16]. Thus, we analysed the activity of RUNX1 by flow cytometric analysis with an anti-phospho RUNX1 (pRUNX1, pS249) antibody.

Knock down of RUNX1 in Jurkat cells decreased the staining of both anti-total RUNX1 and anti- pRUNX1 (Fig. 7A), whereas DM decreased only the staining of anti- pRUNX1 (Fig. 7B and 7C). Time course analysis of pRUNX1 showed that BMP2 increased pRUNX1, while DM suppressed pRUNX1 in stimulated Jurkat cells throughout the experiment (Fig. 7D). Given that RUNX1 activates *IL2* transcription [8] and that pRUNX1 is increased by the activation of RUNX1 [16], these results suggested that BMP signalling regulated IL-2 transcription via activating RUNX1 in T cells.

Discussion

This study provides evidence for the multiple roles of BMP signalling in T-cell activation including IL-2 production, proliferation, and T-cell differentiation. In this paper, some of the evidence was obtained by a small molecule inhibitor of the BMP-SMAD signalling pathway, DM. Therefore, we cannot exclude the possibility that DM directly affects other kinases to achieve the observed effects. However, many effects of DM are related to the reported effects of BMP or other related genes. First, DM inhibited known targets of BMP signalling including SMAD1/5/8. Second, DM suppressed the transcription of *IL2*, a RUNX1-target gene [15]. Consistently, we have found that BMP signalling increased the level of phorsphorylation of RUNX1 protein, while DM decreased it. Moreover, both DM and the extracellular BMP antagonist Noggin inhibited IL-2 production by Jurkat cells, demonstrating that the influence of DM on *IL2* transcription is by inhibition of endogenous BMP signalling. Third, DM suppressed proliferation of T cells. In fact, previous reports have suggested that BMPs regulate T-cell proliferation. BMP4 and BMP6 have been reported to increase proliferation, while BMP2 decreased proliferation [17, 18]. Considering the diversity of BMP ligands and receptors, DM may have a profound effect on T-cell proliferation by inhibiting BMP signal transduction via a wide range of BMP ligands and receptors.

DM differentially affected Th differentiation, relatively unaffecting or even augmenting Th2 differentiation, while suppressing Th17 and iTreg cell differentiation, especially in the early phase of the culture, when DM is thought to have the maximal activity in vitro. Although the differentiation of IFN-γ producing cells in the Th1 conditions was more obviously suppressed by DM in the later phase (d4 and 8) of the culture, the decrease of *Tbx21* by DM at 12 h after stimulation suggests that Th1 differentiation is in fact affected. These results collectively indicate that the effects of DM are not simply the results of the inhibition of all TCR signalling and/or the suppression of the expression of the lineage-specific transcription factors. Rather, it is more likely that DM differentially affects multiple mechanisms in T-cell activation and differentiation.

The suppression of proliferation and differentiation by DM was very remarkable at higher doses ($IC_{50} \sim 5$ μM). However, the doses are above IC_{50} of DM on AMP activated kinase and vascular endothelial growth factor kinase [19], although it is not known whether these kinases have significant roles in T cells. Besides, recombinant Noggin did not have remarkable effects in suppressing proliferation and differentiation (data not shown). Therefore, we do not exclude the possibility that the inhibition of proliferation and differentiation was due to disturbing not only BMP signalling but also other signalling. Yet, it is an interesting finding that low doses of DM mildly increased proliferation (Fig. 2A and B), suggesting that mild and specific inhibition of BMP signalling increased proliferative activity. The multiphasic effect of BMP signalling at low doses of DM was more clearly observed in IL-2 production in Jurkat cells, although this needs to be addressed by more sensitive means. Importantly, DM suppressed IL-2 production in mouse $CD4^+$ T cells in low doses with an IC_{50} similar to the one for the phosphorylation of Smad1/5/8, suggesting that IL-2 was a direct target of the BMP-SMAD signalling in these cells.

The analysis of RUNX1 and phospho-RUNX1 proteins suggests that RUNX1 is an important downstream target of BMP signalling in T cells. The level of the phosphorylated form, but not the total amount, of RUNX1 was decreased at the high dose of DM (5 μM, Fig. 7), where IL-2 production was profoundly suppressed (Fig. 6). We previously reported that RUNX1 was involved in IL-2 transcription, and that knockdown of RUNX1 completely suppressed IL-2 production in Jurkat cells [15]. Thus, it is interesting that the suppression of IL-2 by DM is coupled with the decrease of the phosphorylated form of RUNX1. Also, this result

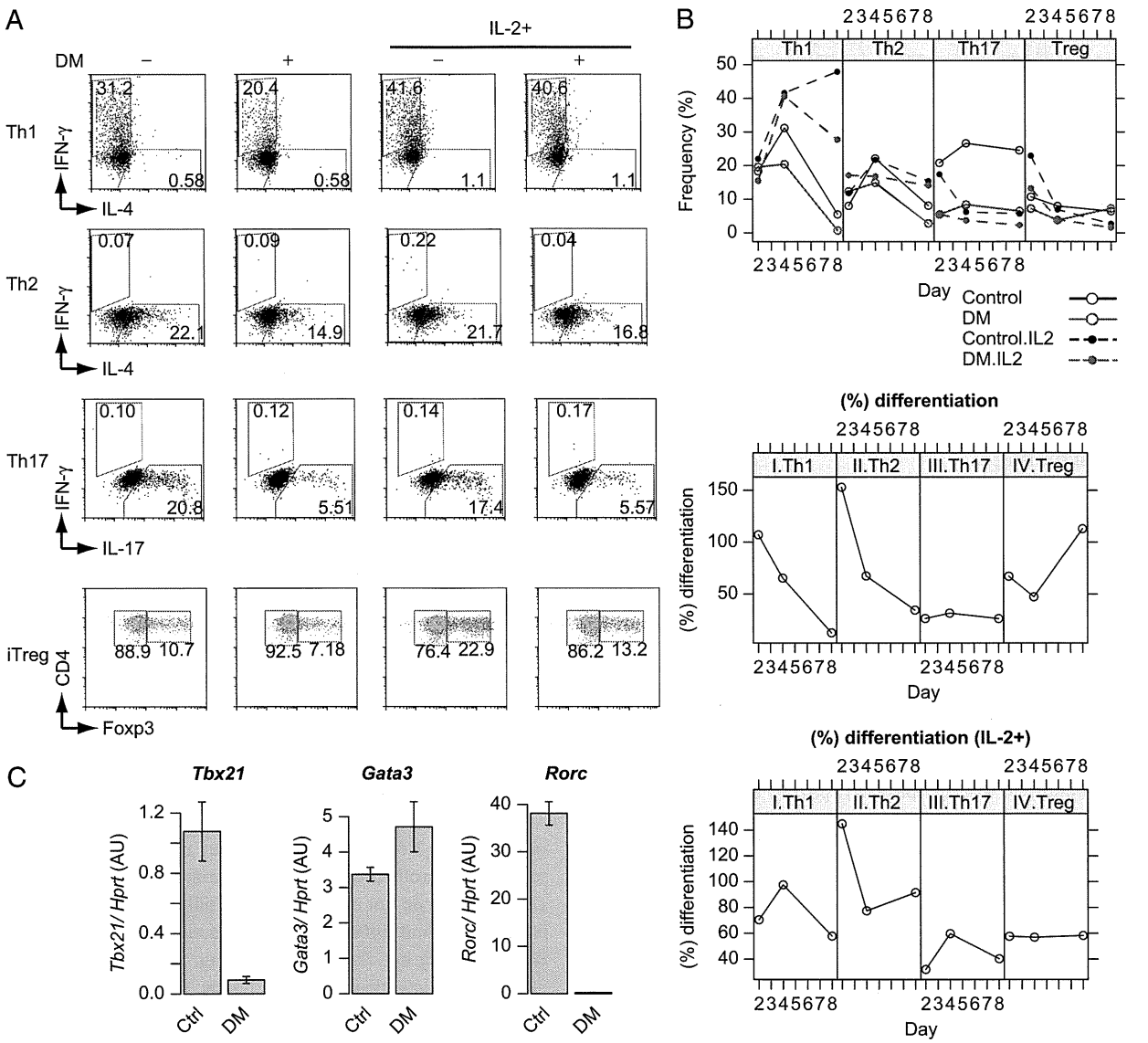

Figure 5. Perturbation effects of DM on Th/Treg differentiation. (A) $CD4^+CD25^-$ T cells were cultured with APCs and soluble anti-CD3 antibody, with DM (5 μM) or DMSO as a control, under indicated polarization conditions for 4 days. Cells were then restimulated with PMA and ionomycin for last 6 h, stained for intracellular cytokines, and analysed by flow cytometry. (B) Time course analysis of Th/Treg differentiation of DM-treated T cells. The frequency of polarized T cells (top), and % differentiation (middle and bottom) are shown. The latter is the value normalized to the percentage of control cells. For the gating strategy, see Supporting Information Fig. 1B. (C) Expression of the lineage-specific transcription factors. $CD4^+CD25^-$ naïve T cells were cultured with DM or DMSO as a control under the indicated conditions for 12 h, and levels of *Tbx21*, *GATA3*, *RORC* were measured by qPCR. *HPRT* was used as a reference gene. Data are shown as mean ± SD of triplicates. Representative results of three (A, B) or two (C) independent experiments are shown.

suggests that the phosphorylated form of RUNX1 is its activated form as suggested by a previous study [16]. Although we cannot exclude the possibility that DM directly suppressed nuclear kinases that phosphorylate RUNX1, this seems unlikely, given that rBMP2 upregulated the level of p-RUNX1 (Fig. 7D). The fact that treatment with rNoggin suppressed IL-2 production in the absence of rBMP2 indicates that in Jurkat cells endogenous BMP secretion signals for IL-2 production. Our study suggests that RUNX1 integrates the milieu of BMPs and its related proteins including Noggin via receiving BMP signalling.

Although further studies are required, BMP ligands and related morphogens from APCs may make morphogen milieus to modulate the differentiation and activation processes of T cells. Previous reports indicate that BMP-2, -4 and -7, and its endogenous inhibitors, Noggin and Chordin, are expressed in thymic epithelial cells

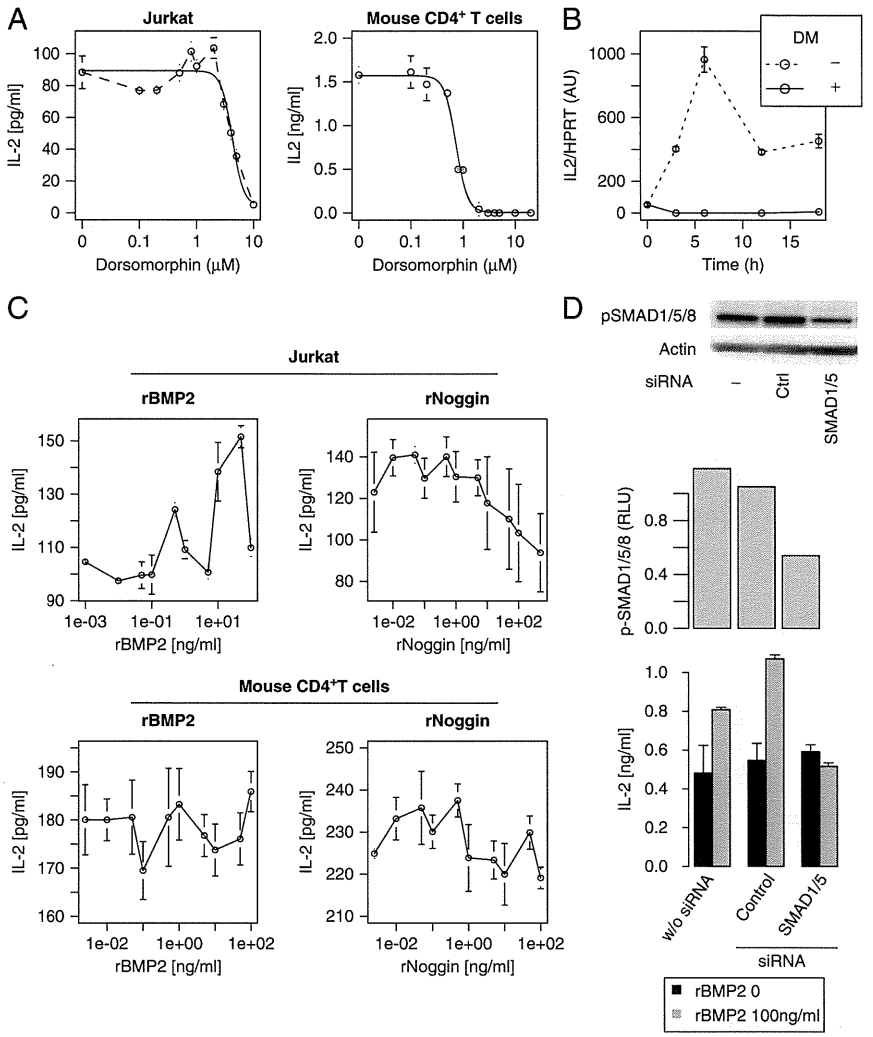

Figure 6. IL-2 production and transcription in DM-treated T cells. (A) Jurkat or mouse CD4$^+$ T cells were cultured for 18 h with DM or DMSO as a control, anti-CD3 and -CD28 antibodies. Data were regressed to a four-parameter log-logistic function (solid line). Points at low doses of DM in Jurkat cells were poorly fit to the log-logistic function, as demonstrated by dashed line. (B) Jurkat cells were stimulated for 3–18 h by anti-CD3 and -CD28 antibodies with DM (5 μM) or DMSO as a control. Relative levels of *Il2* were measured by qPCR. (C) Jurkat or mouse CD4$^+$ T cells were stimulated for 18 hours by anti-CD3 and -CD28 antibodies with titrated doses of recombinant BMP2 protein (rBMP2) or recombinant Noggin protein (rNoggin). IL-2 concentration in the culture supernatant was measured by ELISA. (D) IL-2 production by untreated cells (w/o siRNA) and siRNA-transduced Jurkat cells (control or SMAD1/5-siRNA) with or without rBMP2. Western blotting of pSMAD1/5/8 and actin using siRNA-transduced and non-transduced cells is shown (top). Densitometric analysis of the results of Western blotting of pSMAD1/5/8 and actin is shown (middle). IL-2 production of siRNA-transduced and non-transduced cells with or without rBMP2 (100 ng/mL) is shown (bottom). Data are shown as mean ± SD of triplicates. Representative results of three (A, B) or two (C, D) independent experiments are shown.

[2, 3]. We have found that some BMP ligands and their antagonists are expressed by various immunocytes. For example, monocytes express significantly higher amounts of Chordin (*Chrd*) mRNA than all other cell populations analysed in the data set of T cells, B cells, NK cells, Granulocytes, monocytes, and hematopoietic stem cells (GSE6506, [20]). Also, among B cells, plasma cells express much higher amounts of *Bmp1* and *Gdf2* compared with naïve B cells in the data set GSE4142 [21]. Further studies are required to find biological significance of the expression of these genes and understand the morphogen milieus in the immune system and their influence on T-cell differentiation in vivo.

In conclusion, we show that BMP signalling is involved in T-cell function and differentiation. DM, a specific inhibitor of BMPR (which does not inhibit TGF-β signalling) suppressed specific processes in T-cell activation and differentiation, and induced unique processes in treated cells. We described differential effects of DM and Noggin on T-cell activation and differentiation, demonstrating a physiological role for BMP signalling in these processes

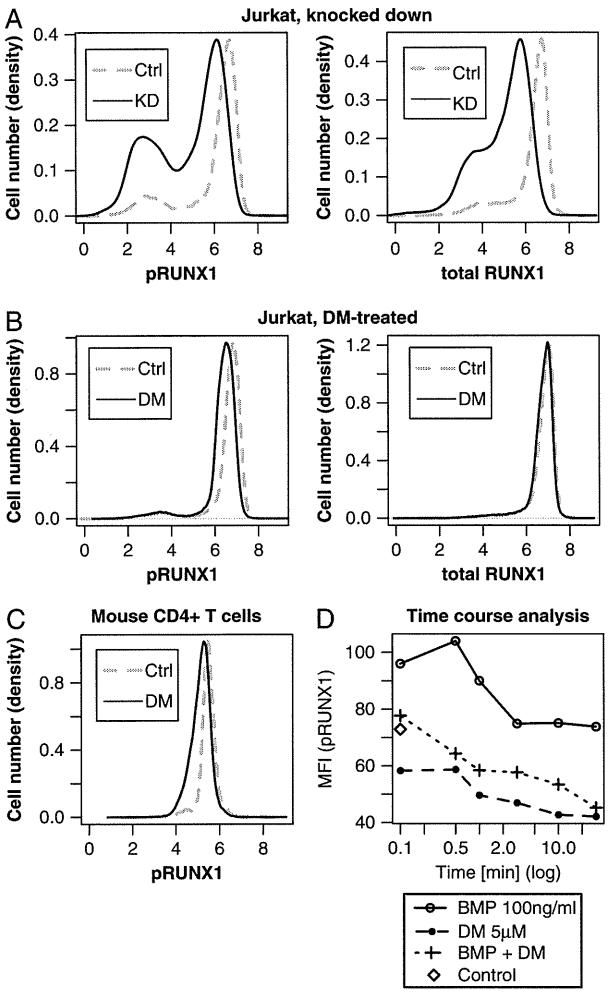

Figure 7. Regulation of phosphorylation of RUNX1/AML1 by BMP signalling. (A) Validation of anti-phospho-RUNX1 (pRUNX1) and -total RUNX1 antibodies. Jurkat cells were transduced with either RUNX1-siRNA (KD) or control siRNA (Ctrl) and cultured for 48 h. Knocked down cells were intracellularly stained by either anti-pRUNX1 or -total RUNX1 antibodies, and subsequently analysed by flow cytometry. (B) Jurkat cells were cultured for 3 h with DM (DM) or DMSO as a control (Ctrl), and subsequently stained by either anti-pRUNX1 or anti-total RUNX1 antibodies. (C) Mouse $CD4^+$ T cells were cultured for 3 h with DM or DMSO as a control, and stained by anti-pRUNX1 antibody. (D) Time course analysis of levels of pRUNX1 in Jurkat cells with rBMP2 and DM or DMSO. Jurkat cells were treated with rBMP2 (100 ng/mL) and either DM (5 μM) or DMSO, and analysed for pRUNX1. Representative results of two (A–C) or three (D) independent experiments are shown.

Materials and methods

Mouse, culture, and cell sorting

BALB/c mice were purchased from Japan SLC (Shizuoka, Japan), maintained under specific pathogen-free conditions in accordance with our institutional guidelines for animal welfare, and were used between 5 and 8 wks of age. $CD4^+$ T cells were isolated and cultured as previously described [15]. For CFSE dilution assay, magnetically sorted mouse $CD25^-CD4^+$ T cells were labeled with 3 μM CFSE (Dojindo and Invitrogen). Irradiated, magnetically sorted mouse $CD4^-CD90.2^-$ cells were used as APCs. DM was purchased from Calbiochem (San Diego).

Quantitative real-time PCR

Total RNA extracted and quantitated as previously described [15]. Primers used for human samples are the followings: *IL-2*, forward: 5′-TGCAACTCCTGT CTTGCATT-3′, reverse: 5′-TCCTG-GTGAGTTT GGGATTC-3′. *HPRT*, forward: 5′-GCTGAGGAT TTG-GAAAGGGTG-3′, reverse: 5′-TGAGCACAC AGAGGGCTACAATG-3′. Primers used for mouse sample are the followings: *Il2*, forward: 5′-CCTGAGCAGGATGGAGAATTACA-3′, reverse: 5′-TCCAGAACATGCCGCAGAG-3′. *Tbx21*, forward: 5′-CAACAAC-CCCTTTGCCAA AG-3′, reverse: 5′-TCCCCCAAGCAGTTGACAG T-3′. *Gata3*, forward: 5′-AGAACCGGCCCCTTA TGAA-3′, reverse: 5′-AGTTCGCGCAGGATGT CC-3′. *Rorc*, forward: 5′-ACCTCCA-CTGCCA GCTGTGTGCTGTC-3′, reverse: 5′-TCATTTCT GCACTT-CTGCATGTAGACTGTC-3′. *HPRT*, forward: 5′-TGAAGAGCTACT-GTAATGATC AGTCAAC-3′, reverse: 5′-AGCAAGCTTGCAAC CTT-AACCA-3′

Western blotting and ELISA

Western blotting and ELISA were preformed as previously described [15]. The following antibodies were used for immunoblot: anti-phospho SMAD1/5/8 (Cell Signallng Technology, Danvers, MA, USA), anti- SMAD1 (Millipore, Billerica, MA, USA), anti-phospho SMAD2 (Cell Signaling Technology), anti-SMAD2/3 (Cell Signaling Technology), anti- $p27^{Kip1}$ (BD Bioscience, San Jose, CA, USA), or anti- Actin (Millipore). IL-2 was measured by ELISA with BD OptEIA™, Human IL-2 ELISA (BD) or Mouse IL-2 ELISA (eBiosciene, San Diego, CA, USA)

Flow cytometric analysis of cell cycle and apoptosis

Cells were fixed with 70% ethanol, denatured, and stained with 7-Amino-actinomycin D (7AAD, Beckman Coulter, Brea, CA, USA), FITC Mouse IgG1k isotype control (MOPC-21, BD Pharmingen), FITC Mouse Anti-BrdU, (3D4, BD Pharmingen). For Annexin staining, cells were stained with Annexin V-FITC (Beckman Coulter), and 7AAD, according to manufacturer's instructions

Flow cytometric analysis of RUNX1

Anti-human and mouse phospho-AML1/RUNX1 (pS249, M93-568.4.27) and anti-human AML1/RUNX1 (N11- 683.51.51) are

generous gifts from BD Pharmingen. Cells were fixed and stained by using Fixation/Permeabilization concentrate (eBioscience), and were subsequently analysed by flow cytometry

Knockdown of AML1/RUNX1 and SMAD1/5

For AML1/RUNX1, Jurkat cells were transduced with AML1/RUNX1 siRNA (Stealth Select RNAi™ siRNA, Invitrogen) or control siRNA (Stealth RNAi™ siRNA Negative Control Hi GC) by the Amaxa nucleofector system according to the manufacturer's instruction. Transduced cells were cultured for 48 hours in the medium, and were subsequently stimulated for 3 h with plate-bound anti-CD3- and soluble anti-CD28-antibodies. Subsequently, cells were stained by either anti-AML1/RUNX1 or anti-phospho-AML1/RUNX1 (by anti-phospho- AML1/RUNX1 only in murine T cells), and were analysed by flow cytometry. For knockdown of SMAD1/5, Jurkat cells were transduced with a mixed siRNA for SMAD1 and SMAD5 (Stealth Select RNAi™) or control siRNA (Stealth RNAi™ siRNA Negative Control Lo GC)

Time course analysis of phopho-AML1/RUNX1

Cells were pre-heated in 2% FCS/PBS at 37°C for 3 min. Subsequently, recombinant BMP2 protein (100 ng/mL), and/or DM (5 μM), or DMSO, were added, and cells were incubated for indicated times. Immediately after incubation, cells were dipped in pre-warmed fixation buffer (BD Phosflow Fix Buffer I, BD bioscience), and incubated for 10 min in 37°C. Subsequently, cells were placed on ice for 30 min. Control cells were prepared with neither BMP2 nor DM, but with an equivalent amount of DMSO, and were fixed for 10 min in 37°C. Cells were permeabilised with chilled (−20°C) buffer (BD Phosflow Perm III Buffer, BD Bioscience) and stained with antibodies

Th/Treg polarization

Freshly sorted mouse $CD25^{-}CD4^{+}$ T cells (5×10^4) were co-cultured with APC (1×10^5) in the presence of 0.5 μg/mL soluble anti-CD3 monoclonal antibody (mAb). In addition, the following pairs of recombinant cytokines (20 ng/mL) and monoclonal mAbs (10 μg/mL) were added: rIL-12 and anti-IL-4 mAb For Th1; rIL-4, anti (IFNL-γ mAb for Th2; rIL-1β, rIL-6, rTGFβ, anti IL-4 mAb, and anti IFN-γ mAb for Th17; TGFL-β and rIL-2 (100 IU/mL, generous gift from Shionogi) for iTreg. Cytokines and Foxp3 were stained as previously described [15]

Microarray analysis

Mouse $CD4^{+}$ T cells were prepared and cultured with or without stimulation by plate bound anti-CD3 mAb and soluble anti-CD28 mAb for 1 h. Subsequently, 4 μM DM or DMSO was added and cells were incubated for 6 h. Total RNA was isolated as previously described [15]. Microarray data are available from the NCBI Gene Expression Omnibus (GEO) repository under the series accession number GSE27378

Bioinformatics for flow cytometric data

Flow cytometric data in Fig. 3A were processed by *flowCore* [22]. Data were normalised for the FL2 channel data (7AAD) by *flowStats* [23], using all the control and experimental groups stained with 7AAD and with or without BrdU-FITC. *FlowStats* normalises FCS data by adjusting the peaks of the channel data used for normalisation. By this normalisation process, the variance of the biphasic signals of 7AAD between samples was minimised without affecting FL1 data, thus enabling exactly same gating for G0/1, S, M, and subG0 in all the samples analysed. Normalised data were visualised by *flowViz* [24]. For CFSE data in Fig. 2, flowJo was used for model fit. The Mann–Whitney *U*-test was used for comparing unpaired flow cytometric data of two groups

Analysis of dose–response curve

Chemiluminescence intensities were quantified by *ImageJ*. Regression analysis for dose response curve was performed by the CRAN package *drc* [25]. Dose response data were fit to the four-parameter log-logistic function, *LL.4* in *drc*, by the following equation (x is the dose).

$$f(x,a,b,c,d) = c + \frac{d-c}{1+e^{b(\log(x)-\log(a))}}$$

Acknowledgements: We would like to give our thanks to Prof. Tessa Crompton for discussion, advice, and critical reading of the manuscript, Prof. Robin Callard, Dr. Tomoyuki Yamaguchi, and Dr. Takashi Nomura for comments on the manuscript. This work was supported by Grant-in-Aid for Specially Promoted Research, and grants-in-aid for Scientific Research on Priority Areas from the Ministry of Education, Culture, Sports, Science and Technology of Japan. MO is a Human Frontier Science Program Long-Term Fellow.

Conflict of interest: The authors declare no commercial or financial conflict of interest.

References

1 **Chen, D., Zhao, M. and Mundy, G. R.,** Bone morphogenetic proteins. *Growth Factors* 2004. **22**: 233–241.

2 **Hager-Theodorides, A. L., Outram, S. V., Shah, D. K., Sacedon, R., Shrimpton, R. E., Vicente, A., Varas, A. et al.,** Bone morphogenetic protein 2/4 signaling regulates early thymocyte differentiation. *J. Immunol.* 2002. **169**: 5496–5504.

3 **Graf, D., Nethisinghe, S., Palmer, D. B., Fisher, A. G. and Merkenschlager, M.,** The developmentally regulated expression of Twisted gastrulation reveals a role for bone morphogenetic proteins in the control of T-cell development. *J. Exp. Med.* 2002. **196**: 163–171.

4 **Lu, L., Ma, J., Wang, X., Wang, J., Zhang, F., Yu, J., He, G. et al.,** Synergistic effect of TGF-b superfamily members on the induction of Foxp3$^+$ Treg. *Eur. J. Immunol.* 2010. **40**: 142–152.

5 **Kawabata, M., Imamura, T. and Miyazono, K.,** Signal transduction by bone morphogenetic proteins. *Cytokine Growth Factor Rev.* 1998. **9**: 49–61.

6 **Miyazono, K., Maeda, S. and Imamura, T.,** BMP receptor signaling: transcriptional targets, regulation of signals, and signaling cross-talk. *Cytokine Growth Factor Rev.* 2005. **16**: 251–263.

7 **Lee, K. S., Kim, H. J., Li, Q. L., Chi, X. Z., Ueta, C., Komori, T., Wozney, J. M. et al.,** Runx2 is a common target of transforming growth factor b1 and bone morphogenetic protein 2, and cooperation between Runx2 and Smad5 induces osteoblast-specific gene expression in the pluripotent mesenchymal precursor cell line C2C12. *Mol. Cell. Biol.* 2000. **20**: 8783–8792.

8 **Pimanda, J. E., Donaldson, I. J., de Bruijn, M. F., Kinston, S., Knezevic, K., Huckle, L., Piltz, S. et al.,** The SCL transcriptional network and BMP signaling pathway interact to regulate RUNX1 activity. *Proc. Natl. Acad. Sci. USA* 2007. **104**: 840–845.

9 **Lee, K. S., Hong, S. H. and Bae, S. C.,** Both the Smad and p38 MAPK pathways play a crucial role in Runx2 expression following induction by transforming growth factor-beta and bone morphogenetic protein. *Oncogene* 2002. **21**: 7156–7163.

10 **Hong, C. C. and Yu, P. B.,** Applications of small molecule BMP inhibitors in physiology and disease. *Cytokine Growth Factor Rev.* 2009. **20**: 409–418.

11 **Yu, P. B., Hong, C. C., Sachidanandan, C., Babitt, J. L., Deng, D. Y., Hoyng, S. A., Lin, H. Y. et al.,** Dorsomorphin inhibits BMP signals required for embryogenesis and iron metabolism. *Nat. Chem. Biol.* 2008. **4**: 33–41.

12 **Rudd, C. E.,** Cell cycle 'check points' T-cell anergy. *Nat. Immunol.* 2006. **7**: 1130–1132.

13 **Bindea, G., Mlecnik, B., Hackl, H., Charoentong, P., Tosolini, M., Kirilovsky, A., Fridman, W. H. et al.,** ClueGO: a Cytoscape plug-in to decipher functionally grouped gene ontology and pathway annotation networks. *Bioinformatics* 2009. **25**: 1091–1093.

14 **Komine, O., Hayashi, K., Natsume, W., Watanabe, T., Seki, Y., Seki, N., Yagi, R. et al.,** The Runx1 transcription factor inhibits the differentiation of naïve CD4$^+$ T cells into the Th2 lineage by repressing GATA3 expression. *J. Exp. Med.* 2003. **198**: 51–61.

15 **Ono, M., Yaguchi, H., Ohkura, N., Kitabayashi, I., Nagamura, Y., Nomura, T., Miyachi, Y. et al.,** Foxp3 controls regulatory T-cell function by interacting with AML1/Runx1. *Nature* 2007. **446**: 685–689.

16 **Aikawa, Y., Nguyen, L. A., Isono, K., Takakura, N., Tagata, Y., Schmitz, M. L., Koseki, H. et al.,** Roles of HIPK1 and HIPK2 in AML1- and p300-dependent transcription, hematopoiesis and blood vessel formation. *EMBO J.* 2006. **25**: 3955–3965.

17 **Sivertsen, E. A., Huse, K., Hystad, M. E., Kersten, C., Smeland, E. B. and Myklebust, J. H.,** Inhibitory effects and target genes of bone morphogenetic protein 6 in Jurkat TAg cells. *Eur. J. Immunol.* 2007. **37**: 2937–2948.

18 **Varas, A., Sacedon, R., Hidalgo, L., Martinez, V. G., Valencia, J., Cejalvo, T., Zapata, A. et al.,** Interplay between BMP4 and IL-7 in human intrathymic precursor cells. *Cell Cycle* 2009. **8**: 4119–4126.

19 **Hao, J., Ho, J. N., Lewis, J. A., Karim, K. A., Daniels, R. N., Gentry, P. R., Hopkins, C. R. et al.,** In vivo structure-activity relationship study of dorsomorphin analogues identifies selective VEGF and BMP inhibitors. *ACS Chem. Biol.* 2010. **5**: 245–253.

20 **Chambers, S. M., Boles, N. C., Lin, K. Y., Tierney, M. P., Bowman, T. V., Bradfute, S. B., Chen, A. J. et al.,** Hematopoietic fingerprints: an expression database of stem cells and their progeny. *Cell Stem Cell* 2007. **1**: 578–591.

21 **Luckey, C. J., Bhattacharya, D., Goldrath, A. W., Weissman, I. L., Benoist, C. and Mathis, D.,** Memory T and memory B cells share a transcriptional program of self-renewal with long-term hematopoietic stem cells. *Proc. Natl. Acad. Sci. USA* 2006. **103**: 3304–3309.

22 **Ellis, B., Haaland, P., Hahne, F., Le Meur, N. and Gopalakrishnan, N., flowCore: Basic structures for flow cytometry data. R *package version* 1.14.1.**

23 **Hahne, F., Gopalakrishnan, N., Khodabakhshi, A. H. and Wong, C. J., flowStats: Statistical methods for the analysis of flow cytometry data. R *package version* 1.6.0.**

24 **Ellis, B., Gentleman, R., Hahne, F., Le Meur, N. and Sarkar, D., flowViz: Visualization for flow cytometry. R *package version* 1.12.0.**

25 **Ritz, C. and Streibig, J. C.,** Bioassay Analysis using R. *J. Stat. Software* 2005. **12**.

Abbreviations: **7AAD:** 7-amino-actinomycin D · **ActRII:** activin type II receptor · **AML1:** acute myeloid leukemia 1 · **BMP:** bone morphogenic protein · **BMPR:** BMP receptor · **DEGs:** differentially expressed genes · **DM:** dorsomorphin · **DN:** double negative · **DP:** double positive · **iTreg:** induced regulatory T cell · **MAPK:** mitogen-activated protein kinase · **qPCR:** quantitative real-time PCR · **rBMP2:** recombinant BMP2 · **rNoggin:** recombinant Noggin · **RUNX1:** runt-related transcription factor 1

Full correspondence: Dr. Masahiro Ono, Immunobiology Unit, Institute of Child Health, University College London, 30 Guilford Street, London WC1N 1EH, UK
Fax: +44-20-7905-2882
e-mail: m.ono@ucl.ac.uk

Received: 28/4/2011
Revised: 7/10/2011
Accepted: 21/11/2011
Accepted article online: 20/12/2011

